

HD-Painter: High-Resolution and Prompt-Faithful Text-Guided Image Inpainting with Diffusion Models

Hayk Manukyan^{1*} Andranik Sargsyan^{1*} Barsegh Atanyan¹ Zhangyang Wang^{1,2}
Shant Navasardyan¹ Humphrey Shi^{1,3}

¹Picsart AI Research (PAIR) ²UT Austin ³Georgia Tech

<https://github.com/Picsart-AI-Research/HD-Painter>



Figure 1. High-resolution (the large side is 2048 in all these examples) text-guided image inpainting results with our approach. The method is able to faithfully fill the masked region according to the prompt even if the combination of the prompt and the known region is highly unlikely. Zoom in to view high-resolution details.

Abstract

Recent progress in text-guided image inpainting, based on the unprecedented success of text-to-image diffusion models, has led to exceptionally realistic and visually plausible results. However, there is still significant potential for improvement in current text-to-image inpainting models, particularly in better aligning the inpainted area with user prompts and performing high-resolution inpainting. There-

fore, in this paper we introduce *HD-Painter*, a completely **training-free** approach that **accurately follows to prompts** and coherently **scales to high-resolution** image inpainting. To this end, we design the Prompt-Aware Introverted Attention (PAIntA) layer enhancing self-attention scores by prompt information and resulting in better text alignment generations. To further improve the prompt coherence we introduce the Reweighting Attention Score Guidance (RASG) mechanism seamlessly integrating a post-hoc sampling strategy into general form of DDIM to prevent out-of-

*Equal contribution.

distribution latent shifts. Moreover, HD-Painter allows extension to larger scales by introducing a specialized super-resolution technique customized for inpainting, enabling the completion of missing regions in images of up to 2K resolution. Our experiments demonstrate that HD-Painter surpasses existing state-of-the-art approaches qualitatively and quantitatively, achieving an impressive generation accuracy improvement of **61.4%** vs **51.9%**. We will make the codes publicly available at: <https://github.com/Picsart-AI-Research/HD-Painter>.

1. Introduction

The recent wave of diffusion models [12, 34] has taken the world by storm, becoming an increasingly integral part of our everyday lives. After the unprecedented success of text-to-image models [26, 27, 30, 37, 41] diffusion-based image manipulations such as prompt-conditioned editing and variations [3, 11, 41], controllable generation [19, 39, 45], object-level image editing [10], personalized and specialized image synthesis [9, 18, 29], multimodal [41] etc. became hot topics in computer vision leading to a huge amount of applications. Particularly, text-guided image completion or inpainting [1, 36, 37] allows users to generate new content in user-specified regions of given images based on textual prompts (see Fig. 1), leading to use cases like retouching specific areas of an image, replacing or adding objects, and modifying subject attributes such as clothes, colors, or emotion.

Pretrained text-to-image generation models such as Stable Diffusion [27], Imagen [30], and Dall-E 2 [26] can be adapted for image completion by blending diffused known regions with generated (denoised) unknown regions during the backward diffusion process. Although such approaches [1, 2] produce well-harmonized and visually plausible completions, they lack global scene understanding especially when denoising in high diffusion timesteps.

To address this, existing methods [22, 27, 36, 38] modify pretrained text-to-image models to take additional context information and fine-tune specifically for text-guided image completion. GLIDE ([22]) and Stable Inpainting (inpainting method fine-tuned on Stable Diffusion) concatenate the mask and the masked image as additional channels to the input of the diffusion UNet, initializing the new convolutional weights with zeros. Furthermore, to get better mask alignment, SmartBrush [38] utilizes instance-aware training with object bounding boxes and segmentation masks.

Despite the mentioned approaches yielding high-quality generation with impressive diversity and realism, we noticed a major drawback of *prompt neglect* expressed by two scenarios: (i) *Background dominance*: when the unknown region is completed with the background ignoring the prompt (e.g. Fig. 4, rows 1, 3), and (ii) *nearby object*

dominance: when the known region objects are propagated to the unknown region according to the visual context likelihood rather than the given prompt (e.g. Fig. 4, rows 5, 6).

Perhaps both issues arise because the vanilla diffusion inpainting lacks the capability to accurately interpret the textual prompt or combine it with the contextual information from the known region. To address the mentioned problems we introduce *Prompt-Aware Introverted Attention (PAIntA)* block without any *training or fine-tuning* requirements. PAIntA enhances the self-attention scores according to the given textual condition aiming to decrease the impact of non-prompt-relevant information from the image known region while increasing the contribution of the prompt-aligned known pixels.

To improve the text-alignment of the generation results even further we apply a *post-hoc guidance* mechanism by leveraging the cross-attention scores. However the vanilla post-hoc guidance mechanism used by seminal works such as [6, 7], etc. may lead to generation quality degradation due to out-of-distribution shifts caused by the additional gradient term in the backward diffusion equation (see Eq. 4). To this end we propose *Reweighting Attention Score Guidance (RASG)*, a post-hoc mechanism seamlessly integrating the gradient component in the general form of DDIM process. This allows to simultaneously guide the sampling towards more prompt-aligned latents and keep them in their trained domain leading to visually plausible inpainting results.

With the combination of PAIntA and RASG our method gains a significant advantage over the current state-of-the-art approaches by solving the issue of prompt neglect. Moreover PAIntA and RASG both are plug-and-play components so can be added on top of any diffusion base inpainting model to alleviate the mentioned problem. In addition, by leveraging high-resolution diffusion models and time-iterative blending technology we design a simple yet effective pipeline for up to 2048×2048 resolution inpainting.

To summarize, our main contributions are as follows:

- We introduce the *Prompt-Aware Introverted Attention (PAIntA)* layer to alleviate the prompt neglect issues of background and nearby object dominance in text-guided image inpainting.
- To further improve the text-alignment of generation we present the *Reweighting Attention Score Guidance (RASG)* strategy which enables to prevent out-of-distribution shifts while performing post-hoc guided sampling.
- Our designed pipeline for text-guided image completion is *completely training-free* and demonstrates a significant advantage over current state-of-the-art approaches quantitatively and qualitatively. Moreover, with the additional

help of our simple yet effective inpainting-specialized super-resolution framework we make high-resolution (up to 2048×2048) image completion possible.

2. Related Work

2.1. Image Inpainting

Image inpainting is the task of filling missing regions of the image in a visually plausible manner. Early deep learning approaches such as [20, 42, 43] introduce mechanisms to propagate deep features from known regions. Later [31, 40, 46, 47] utilize StyleGAN-v2-like [14] decoder and discriminative training for better image detail generation.

After diffusion models have been introduced the inpainting task also benefited from them. Particularly text-guided image inpainting approaches emerged. Given a pre-trained text-to-image diffusion model [1, 2] replace the unmasked region of the latent by the noised version of the known region during sampling. However, as noted by [22], this leads to poor generation quality, as the denoising network only sees the noised version of the known region. Therefore they propose fine-tuning pretrained text-to-image models for text-guided image inpainting by conditioning the denoising model on the unmasked region and a generated random mask via concatenation. [38] incorporates object-mask prediction into training to get better mask alignment. In this work we propose a training-free approach leveraging plug-and-play components PAIntA and RASG, and improving the text-prompt alignment. Moreover, our approach allows inpainting on high-resolution images (up to 2048×2048).

2.2. Inpainting-Specific Architectural Blocks

Early deep learning approaches were designing special layers for better/more efficient inpainting. Particularly, [17, 20, 44] introduce special convolutional layers dealing with the known region of the image to effectively extract the information useful for visually plausible image completion. [42] introduces the contextual attention layer reducing the unnecessarily heavy computations of all-to-all self-attention for high-quality inpainting. In this work we propose Prompt-Aware Introverted Attention (PAIntA) layer, specifically designed for text-guided image inpainting. It aims to decrease (increase) the prompt-irrelevant (-relevant) information from the known region for better text aligned inpainting generation.

2.3. Post-Hoc Guidance in Diffusion Process

Post-hoc guidance methods are backward diffusion sampling techniques which guide the next step latent prediction towards a specific objective function minimization. Such approaches appear to be extremely helpful when generating visual content especially with an additional constraint. Particularly [6] introduced classifier-guidance aim-

ing to generate images of a specific class. Later CLIP-guidance was introduced by [22] leveraging CLIP [25] as an open-vocabulary classification method. LDM [27] further extends the concept to guide the diffusion sampling process by any image-to-image translation method, particularly guiding a low-resolution trained model to generate $\times 2$ larger images. [4] guides image generation by maximizing the maximal cross-attention score relying on multi-iterative optimization process resulting in more text aligned results. [7] goes even further by utilizing the cross-attention scores for object position, size, shape, and appearance guidances. All the mentioned post-hoc guidance methods shift the latent generation process by a gradient term (see Eq. 6) sometimes leading to image quality degradations.

To this end we propose the Reweighting Attention Score Guidance (RASG) mechanism allowing to perform post-hoc guidance with any objective function **while preserving the diffusion latent domain**. Specifically for inpainting task, to alleviate the issue of prompt neglect, we benefit from a guidance objective function based on the open-vocabulary segmentation properties of cross-attentions.

3. Method

We first formulate the text-guided image completion problem followed by an introduction to diffusion models, particularly Stable Diffusion ([27]) and Stable Inpainting. We then discuss the overview of our method and its components. Afterwards we present our Prompt-Aware Introverted Attention (PAIntA) block and Reweighting Attention Score Guidance (RASG) mechanism in detail. Lastly our inpainting-specific super-resolution technique is introduced.

Let $I \in \mathbb{R}^{H \times W \times 3}$ be an RGB image, $M \in \{0, 1\}^{H \times W}$ be a binary mask indicating the region in I one wants to inpaint with a textual prompt τ . The goal of text-guided image inpainting is to output an image $I^c \in \mathbb{R}^{H \times W \times 3}$ such that I^c contains the objects described by the prompt τ in the region M while outside M it coincides with I , i.e. $I^c \odot (1 - M) = I \odot (1 - M)$.

3.1. Stable Diffusion and Stable Inpainting

Stable Diffusion (SD) is a diffusion model that functions within the latent space of an autoencoder $\mathcal{D}(\mathcal{E}(\cdot))$ (VQ-GAN [8] or VQ-VAE [35]) where \mathcal{E} denotes the encoder and \mathcal{D} the corresponding decoder. Specifically, let $I \in \mathbb{R}^{H \times W \times 3}$ be an image and $x_0 = \mathcal{E}(I)$, consider the following forward diffusion process with hyperparameters $\{\beta_t\}_{t=1}^T \subset [0, 1]$:

$$q(x_t|x_{t-1}) = \mathcal{N}(x_t; \sqrt{1 - \beta_t}x_{t-1}, \beta_t I), \quad t = 1, \dots, T \quad (1)$$

where $q(x_t|x_{t-1})$ is the conditional density of x_t given x_{t-1} , and $\{x_t\}_{t=0}^T$ is a Markov chain. Here T is large

enough to allow an assumption $x_T \sim \mathcal{N}(\mathbf{0}, \mathbf{1})$. Then SD learns a backward process (below similarly, $\{x_t\}_{t=T}^0$ is a Markov chain)

$$p_\theta(x_{t-1}|x_t) = \mathcal{N}(x_{t-1}; \mu_\theta(x_t, t), \sigma_t \mathbf{1}), \quad t = T, \dots, 1, \quad (2)$$

and hyperparameters $\{\sigma_t\}_{t=1}^T$, allowing the generation of a signal x_0 from the standard Gaussian noise x_T . Here $\mu_\theta(x_t, t)$ is defined by the predicted noise $\epsilon_\theta^t(x_t)$ modeled as a neural network (see [12]): $\mu_\theta(x_t, t) = \frac{1}{\sqrt{\beta_t}} \left(x_t - \frac{\beta_t}{\sqrt{1-\alpha_t}} \epsilon_\theta^t(x_t) \right)$. Then $\hat{I} = \mathcal{D}(x_0)$ is returned.

The following claim can be derived from the main DDIM principle, Theorem 1 in [34].

CLAIM 1 *After training the diffusion backward process (Eq. 2) the following $\{\sigma_t\}_{t=1}^T$ -parametrized family of DDIM sampling processes can be applied to generate high-quality images:*

$$x_{t-1} = \sqrt{\alpha_{t-1}} \frac{x_t - \sqrt{1-\alpha_t} \epsilon_\theta^t(x_t)}{\sqrt{\alpha_t}} + \sqrt{1-\alpha_{t-1} - \sigma_t^2 \epsilon_\theta^t(x_t) + \sigma_t \epsilon_t}, \quad (3)$$

where $\epsilon_t \sim \mathcal{N}(\mathbf{0}, \mathbf{I})$, $\alpha_t = \prod_{i=1}^t (1 - \beta_i)$, and $0 \leq \sigma_t \leq \sqrt{1 - \alpha_{t-1}}$ can be arbitrary parameters.

Usually (e.g. in SD or Stable Inpainting described below) $\sigma_t = 0$ is taken to get a deterministic process:

$$x_{t-1} = \sqrt{\alpha_{t-1}} \left(\frac{x_t - \sqrt{1-\alpha_t} \epsilon_\theta^t(x_t)}{\sqrt{\alpha_t}} \right) + \sqrt{1-\alpha_{t-1}} \epsilon_\theta^t(x_t), \quad t = T, \dots, 1. \quad (4)$$

For text-to-image synthesis, SD guides the processes with a textual prompt τ . Hence the function $\epsilon_\theta^t(x_t) = \epsilon_\theta^t(x_t, \tau)$, modeled by a UNet-like ([28]) architecture, is also conditioned on τ by its cross-attention layers. For simplicity sometimes we skip τ in writing $\epsilon_\theta^t(x_t, \tau)$.

As mentioned earlier, Stable Diffusion can be modified and fine-tuned for text-guided image inpainting. To do so [27] concatenate the features of the masked image $I^M = I \odot (1 - M)$ obtained by the encoder \mathcal{E} , and the (downscaled) binary mask M to the latents x_t and feed the resulting tensor to the UNet to get the estimated noise $\epsilon_\theta^t([x_t, \mathcal{E}(I^M), \text{down}(M)], \tau)$, where *down* is the downscaling operation to match the shape of the latent x_t . Newly added convolutional filters are initialized with zeros while the rest of the UNet from a pretrained checkpoint of Stable Diffusion. Training is done by randomly masking images and optimizing the model to reconstruct them based on image captions from the LAION-5B ([32]) dataset. The resulting model shows visually plausible image completion and we refer to it as *Stable Inpainting*.

3.2. HD-Painter: Overview

The overview of our method is presented in Fig. 2. The proposed pipeline is composed of two stages: text-guided image inpainting on the resolution $H/4 \times W/4$ is applied followed by the inpainting-specific $\times 4$ super-resolution of the generated content.

To complete the missing region M according to the given prompt τ we take a pre-trained inpainting diffusion model like Stable Inpainting, replace the self-attention layers by PAIntA layers, and perform a diffusion backward process by applying our RASG mechanism. After getting the final estimated latent x_0 , it is decoded resulting in an inpainted image $I_{low}^c = \mathcal{D}(x_0) \in \mathbb{R}^{\frac{H}{4} \times \frac{W}{4}}$.

To inpaint the original size image $I \in \mathbb{R}^{H \times W}$ we utilize the super-resolution stable diffusion from [27]. We apply the diffusion backward process of SD starting from $X_T \sim \mathcal{N}(\mathbf{0}, \mathbf{1})$ and conditioned on the low resolution inpainted image I_{low}^c . After each step we blend the denoised X_0^{pred} with the original image's encoding $\mathcal{E}(I)$ in the known region indicated by the mask $(1 - M) \in \{0, 1\}^{H \times W}$ and derive the next latent X_{t-1} by Eq. 4. After the final step we decode the latent by $\mathcal{D}(X_0)$ and use Poisson blending ([23]) with I to avoid edge artifacts.

3.3. Prompt-Aware Introverted Attention (PAIntA)

Throughout our experiments we noticed that existing approaches, such as Stable Inpainting, tend to ignore the user-provided prompt relying more on the visual context around the inpainting area. In the introduction we categorized this issue into two classes based on user experience: *background dominance* and *nearby object dominance*. Indeed, for example in Fig. 4, rows 1, 3, 4, the existing solutions (besides BLD) fill the region with background, and in rows 5, 6, they prefer to continue the animal and the car instead of generating a boat and flames respectively. We hypothesize that the *visual context dominance* over the prompt is attributed to the *prompt-free, only-spatial* nature of self-attention layers. To support this we visualize the self-attention scores (see Appendix) and observe a high similarity between the inpainted tokens and such known tokens of the image which have low similarity with the prompt (for more details see Appendix). Therefore, to alleviate the issue, we introduce a plug-in replacement for self-attention, Prompt-Aware Introverted Attention (PAIntA, see Fig. 3 (a)) which utilizes the inpainting mask M and cross-attention matrices to control the self-attention output in the unknown region. Below we discuss PAIntA in detail.

Let $X \in \mathbb{R}^{(h \times w) \times d}$ be the input tensor of PAIntA. Similar to self-attention, PAIntA first applies projection layers to get the queries, keys, and values we denote by $Q_s, K_s, V_s \in \mathbb{R}^{(h \times w) \times d}$ respectively, and the similarity matrix $A_{self} = \frac{Q_s K_s^T}{\sqrt{d}} \in \mathbb{R}^{hw \times hw}$. Then we mitigate the too strong influence of the known region over the un-

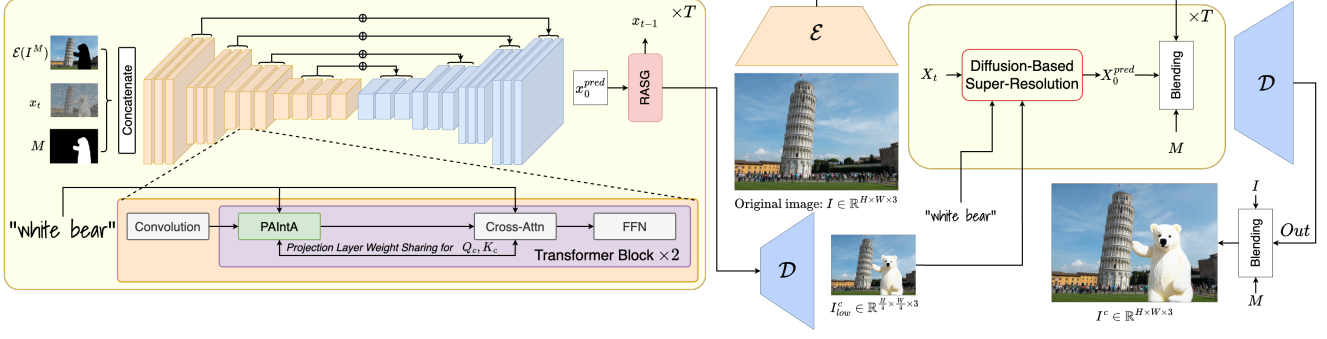


Figure 2. Our method has two stages: image completion, and inpainting-specialized super-resolution ($\times 4$). For image completion in each diffusion step we denoise the latent x_t by conditioning on the inpainting mask M and the masked downsampled image $I^M = \text{down}(I) \odot (1 - M) \in \mathbb{R}^{\frac{H}{4} \times \frac{W}{4} \times 3}$ (encoded with the VAE encoder \mathcal{E}). To make better alignment with the given prompt our PAIntA block is applied instead of self-attention layers. After predicting the denoised x_0^{pred} in each step t , we provide it to our RASG guidance mechanism to estimate the next latent x_{t-1} . For inpainting-specific super resolution we condition the high-resolution latent X_t denoising process by the lower resolution inpainted result I_{low}^c , followed by blending $X_0^{pred} \odot M + \mathcal{E}(I) \odot (1 - M)$. Finally we get I^c by Poisson blending the decoded output with the original image I .

known by adjusting the attention scores of known pixels contributing to the inpainted region. Specifically, leveraging the prompt τ , PAIntA defines a new similarity matrix:

$$\begin{aligned} \tilde{A}_{self} &\in \mathbb{R}^{hw \times hw}, \\ (\tilde{A}_{self})_{ij} &= \begin{cases} c_j \cdot (A_{self})_{ij} & M_i = 1 \text{ and } M_j = 0, \\ (A_{self})_{ij} & \text{otherwise,} \end{cases} \end{aligned} \quad (5)$$

where c_j shows the alignment of the j^{th} feature token (pixel) with the given textual prompt τ .

We define $\{c_j\}_{j=1}^{hw}$ using the cross-attention spatio-textual similarity matrix $S_{cross} = \text{SoftMax}(Q_c K_c^T / \sqrt{d})$, where $Q_c \in \mathbb{R}^{(h \times w) \times d}$, $K_c \in \mathbb{R}^{l \times d}$ are query and key tensors of corresponding cross-attention layers, and l is the number of tokens of the prompt τ . Specifically, we consider CLIP text embeddings of the prompt τ and separate the ones which correspond to the words of τ and *End of Text* (EOT) token (in essence we just disregard the SOT token and the null-token embeddings), and denote the set of chosen indices by $\text{ind}(\tau) \subset \{1, 2, \dots, l\}$. We include EOT since (in contrast with SOT) it contains information about the prompt τ according to the architecture of CLIP text encoder. For each j^{th} pixel we define its similarity with the prompt τ by summing up its similarity scores with the embeddings indexed from $\text{ind}(\tau)$, i.e. $c_j = \sum_{k \in \text{ind}(\tau)} (S_{cross})_{jk}$. Also, we found beneficial to normalize the scores $c_j = \text{clip}\left(\frac{c_j - \text{median}(c_k; k=1, \dots, hw)}{\max(c_k; k=1, \dots, hw)}, 0, 1\right)$, where clip is the clipping operation between $[0, 1]$.

Note that in vanilla SD cross-attention layers come after self-attention layers, hence in PAIntA to get query and key tensors Q_c, K_c we borrow the projection layer weights from the next cross-attention module (see Fig. 2). Finally we get the output of the PAIntA layer with the residual connection

with the input: $\text{Out} = X + \text{SoftMax}(\tilde{A}_{self}) \cdot V_s$.

3.4. Reweighting Attention Score Guidance (RASG)

To further enhance the generation alignment with the prompt τ we adopt a post-hoc sampling guidance mechanism [6] with an objective function $S(x)$ leveraging the open-vocabulary segmentation properties of cross-attention layers. Specifically¹ at each step the following update rule is used after predicting the noise $\epsilon_\theta^t(x_t)$: $\hat{\epsilon}_\theta^t(x_t) \leftarrow \epsilon_\theta^t(x_t) + \sqrt{1 - \alpha_t} \cdot s \nabla_{x_t} S(x_t)$, where s is a hyperparameter controlling the amount of the guidance. However, as also noted by [4], vanilla post-hoc guidance may shift the domain of diffusion latents x_{t-1} resulting in image quality degradations. Indeed, according to the (deterministic) DDIM process (Eq. 4) after substituting $\epsilon_\theta^t(x_t)$ with $\hat{\epsilon}_\theta^t(x_t)$ we get

$$\begin{aligned} x_{t-1} &= \sqrt{\alpha_{t-1}} \frac{x_t - \sqrt{1 - \alpha_t} \epsilon_\theta^t(x_t)}{\sqrt{\alpha_t}} + \\ &\quad \sqrt{1 - \alpha_{t-1}} \epsilon_\theta^t(x_t) - \xi_t \nabla_{x_t} S(x_t), \quad (6) \\ \xi_t &= \sqrt{1 - \alpha_t} \cdot s \left(\frac{\sqrt{1 - \alpha_t} \sqrt{\alpha_{t-1}}}{\sqrt{\alpha_t}} - \sqrt{1 - \alpha_{t-1}} \right), \end{aligned}$$

hence in Eq. 4 we get the additional term $-\xi_t \nabla_{x_t} S(x_t)$ which may shift the original distribution of x_{t-1} .

To this end we introduce the *Reweighting Attention Score Guidance (RASG)* strategy which benefits from the general DDIM backward process (Eq. 3) and introduces a gradient reweighting mechanism resulting in latent domain preservation. Specifically, according to Claim 1, x_{t-1} obtained either by Eq. 4 or by Eq. 3 will be in the required domain (see Fig. 3). Hence if in Eq. 3 we replace the stochastic component ϵ_t by the rescaled version of the gradient $\nabla_{x_t} S(x_t)$ (to

¹for brevity: $\epsilon_\theta^t(x_t) = \epsilon_\theta^t([x_t, \mathcal{E}(I^M), \text{down}(M)], \tau)$.

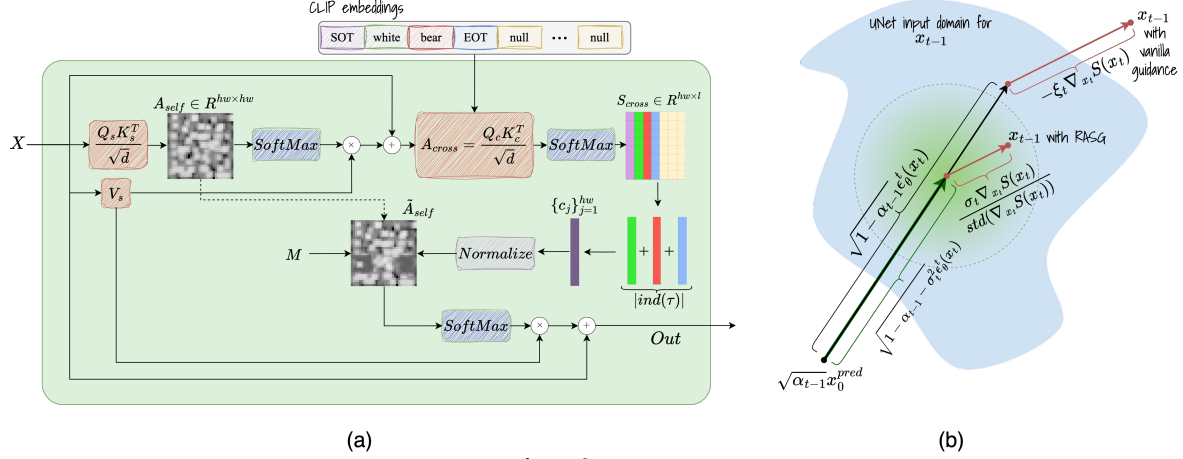


Figure 3. (a) PAIntA block takes an input tensor $X \in \mathbb{R}^{h \times w \times 3}$ and the CLIP embeddings of τ . After computing the self- and cross-attention scores A_{self} and A_{cross} , we update the former (Eq. 5) by scaling with the normalized values $\{c_j\}_{j=1}^{hw}$ obtained from $S_{cross} = \text{SoftMax}(A_{cross})$. Finally the updated attention scores \tilde{A}_{self} are used for the convex combination of the values V_s to get the residual of PAIntA’s output. (b) RASG mechanism takes the predicted scaled denoised latent $\sqrt{\alpha_{t-1}}x_0^{pred} = \frac{\sqrt{\alpha_{t-1}}}{\sqrt{\alpha_t}}(x_t - \sqrt{1 - \alpha_t}\epsilon_\theta(x_t))$ and guides the x_{t-1} estimation process towards minimization of $S(x_t)$ defined by Eq. 9. Gradient reweighting makes the gradient term close to being sampled from $\mathcal{N}(\mathbf{0}, \mathbf{1})$ (green area) by so ensuring the domain preservation (blue area).

make it closer to a sampling from $\mathcal{N}(\mathbf{0}, \mathbf{1})$, we will keep x_{t-1} in the required domain and at the same time will guide its sampling towards minimization of $S(x_t)$. Rescaling of the gradient $\nabla_{x_t} S(x_t)$ is done by dividing it on its standard deviation (we do not change the mean to keep the direction of the $S(x_t)$ minimization, for more discussion see Appendix). Thus, RASG sampling is done by the formula

$$x_{t-1} = \sqrt{\alpha_{t-1}} \frac{x_t - \sqrt{1 - \alpha_t} \epsilon_\theta(x_t)}{\sqrt{\alpha_t}} + \sqrt{1 - \alpha_{t-1} - \sigma_t^2 \epsilon_\theta(x_t) + \sigma_t} \frac{\nabla_{x_t} S(x_t)}{\text{std}(\nabla_{x_t} S(x_t))}. \quad (7)$$

Now let us define the function $S(x_t)$ (for more discussion on its choice see Appendix). First we consider all cross-attention maps A_{cross} with the output resolution of $\frac{H}{32} \times \frac{W}{32}$: $A_{cross}^1, \dots, A_{cross}^m \in \mathbb{R}^{(H/32 \cdot W/32) \times l}$, where m is the number of such cross-attention layers, and l is the number of token embeddings. Then for each $k \in \text{ind}(\tau) \subset \{1, \dots, l\}$ we average the attention maps and reshape to $\frac{H}{32} \times \frac{W}{32}$:

$$\bar{A}_{cross}^k(x_t) = \frac{1}{m} \sum_{i=1}^m A_{cross}^i[:, k] \in \mathbb{R}^{\frac{H}{32} \times \frac{W}{32}}. \quad (8)$$

Using post-hoc guidance with $S(x_t)$ we aim to maximize the attention scores in the unknown region determined by the binary mask $M \in \{0, 1\}^{H \times W}$, hence we take the average binary cross entropy between $\bar{A}^k(x_t)$ and M (M is downsampled with NN interpolation, σ here is sigmoid):

$$S(x_t) = - \sum_{k \in \text{ind}(\tau)} \sum_{i=1}^{\frac{H}{32} \cdot \frac{W}{32}} [M_i \log \sigma(\bar{A}_{cross}^k(x_t)_i) + (1 - M_i) \log(1 - \sigma(\bar{A}_{cross}^k(x_t)_i))]. \quad (9)$$

3.5. Inpainting-Specialized Conditional Super-Resolution

Here we discuss our method for high-resolution inpainting utilizing a pre-trained diffusion-based super-resolution model. We leverage the fine-grained information from the known region to upscale the inpainted region (see Fig. 2.). Recall that $I \in \mathbb{R}^{H \times W \times 3}$ is the original high-resolution image we want to inpaint, and \mathcal{E} is the encoder of VQ-GAN [8]. We consider $X_0 = \mathcal{E}(I)$ and take a standard Gaussian noise $X_T \in \mathbb{R}^{\frac{H}{4} \times \frac{W}{4} \times 4}$. Then we apply a backward diffusion process (Eq. 4) on X_T by using the upscale-specialized SD model and conditioning it on the low resolution inpainted image I_{low}^c . After each diffusion step we blend the estimated denoised latent $X_0^{pred} = (X_t - \sqrt{1 - \alpha_t} \epsilon_\theta^t(X_t)) / \sqrt{\alpha_t}$ with X_0 by using M :

$$X_0^{pred} \leftarrow M \odot X_0^{pred} + (1 - M) \odot X_0, \quad (10)$$

and use the new X_0^{pred} to determine the latent X_{t-1} (by Eq. 4). After the last diffusion step X_0^{pred} is decoded and blended (Poisson blending) with the original image I .

It’s worth noting that our blending approach is inspired by seminal works [1, 33] blending X_t with the noisy latents of the forward diffusion. In contrast, we blend high-

Model Name	CLIP \uparrow	Acc \uparrow	PickScore (Ours vs Baselines) \downarrow
GLIDE	24.92	44.0 %	62.7 %
NUWA-LIP	24.07	31.8 %	67.5 %
BLD	24.81	49.8 %	56.3 %
Stable Inpainting	24.86	51.9 %	54.3 %
Ours	26.34	61.4 %	50.0 %

Table 1. Quantitative comparison

Model Name	CLIP \uparrow	Acc \uparrow
base (Stable Inpainting)	24.86	51.9 %
only PAIntA	25.24	52.2 %
only RASG	25.85	62.0 %
RASG & PAIntA	26.34	61.4 %

Table 2. Ablation study for PAIntA and RASG.

frequencies from X_0 with the denoised prediction X_0^{pred} allowing noise-free image details propagate from the known region to the missing one during all diffusion steps.

4. Experiments

4.1. Implementation Details

Our code is based on the Stable Diffusion 2.0 public GitHub repository from <https://github.com/Stability-AI/stablediffusion> which also includes the Stable Inpainting 2.0 and Stable Super-Resolution 2.0 pre-trained models we use as image completion and inpainting-specialized super-resolution baselines respectively. PAIntA is used to replace the self attention layers on the $H/32 \times W/32$ and $H/16 \times W/16$ resolutions. For RASG we select only cross-attention similarity matrices of the $H/32 \times W/32$ resolution as we noticed no further improvements when taking also finer resolutions (the reason is that the segmentation by cross-attention layers is coarse anyway majorly independent on the layer input resolution) while the diffusion process slows down significantly. For hyperparameters $\{\sigma_t\}_{t=1}^T$ we chose $\sigma_t = \eta\sqrt{(1 - \alpha_{t-1})/(1 - \alpha_t)}\sqrt{1 - \alpha_t/\alpha_{t-1}}$, $\eta = 0.25$.

4.2. Experimental Setup

Here we compare with existing state-of-the-art methods such as GLIDE [22], Stable Inpainting [27], NUWA-LIP [21], and Blended Latent Diffusion (BLD) [2]. We evaluate the methods on a random sample of 10000 (image, mask, prompt) triplets from the validation set of MSCOCO 2017 [16], where the prompt is chosen as the label of the selected instance mask. We noticed that when a precise mask of a recognizable shape is given to Stable Inpainting, it tends to ignore the prompt and inpaint based on the shape. To prevent this, we use the convex hulls of the object segmentation masks and compute the metrics accordingly.

We evaluate the CLIP score on a cropped region of the image using the bounding box of the input mask. As CLIP score can still assign high scores to adversarial examples, we additionally compute the generation class accuracy. So, we utilize a pre-trained instance detection model for MSCOCO: MMDetection [5]. We run it on the cropped area of the generated image, and, as there might be more than one objects included in the crop, we treat the example as positive if the prompt label is in the detected object list.

Finally, we employ PickScore [15] as a combined metric of text-alignment and visual fidelity. Being trained on real user feedback PickScore is able to not only assess the prompt-faithfulness of inpainting methods but also the generation quality, while reflecting the complex requirements of users. In our setting we apply PickScore between our vs other methods results and compute the percentage when it gives the advantage to our.

4.3. Quantitative and Qualitative Analysis

Table 1 shows that our method outperforms the competitors with all three metrics with a large margin. Particularly we improve by more than 1.5 points of CLIP score on top of all competitors, and reached generation accuracy (Acc) of 61.4% vs 51.9 % from other state-of-the-art methods. Furthermore, the PickScore comparison shows our advantage over the competitors in terms of overall quality as well.

We also performed a user study which demonstrates our clear advantage over the competitor state-of-the-art methods in terms of both: *prompt alignment* and *overall quality*. Due to space limitations we present the details of our user study in the supplementary material.

The examples in Fig. 4 demonstrate qualitative comparison between our method and the other state-of-the-art approaches. In many cases the baseline methods either generate a background (Fig. 4, rows 1, 2, 3, 4) or reconstruct the missing regions as continuation of the known region objects disregarding the prompt (Fig. 4, rows 5,6), while our method, thanks to the combination of PAIntA and RASG, successfully generates the target objects. Notice that BLD generates the required object more than other competitors, however the quality of the generation is poor. Similarly, Stable Inpainting sometimes generates the object but the frequency of getting prompt-alignment is low (see Appendix).

Additionally, Fig. 1 demonstrates how effective our inpainting-specialized super-resolution is in seamlessly leveraging known region details for upscaling the generated region. We show more results in our Appendix, as well as comparison with vanilla Stable Super-Resolution approach [27] used as an upscaling method after inpainting.

4.4. Ablation Study

In Table 2 we show that PAIntA and RASG separately on their own provide substantial improvements to the model

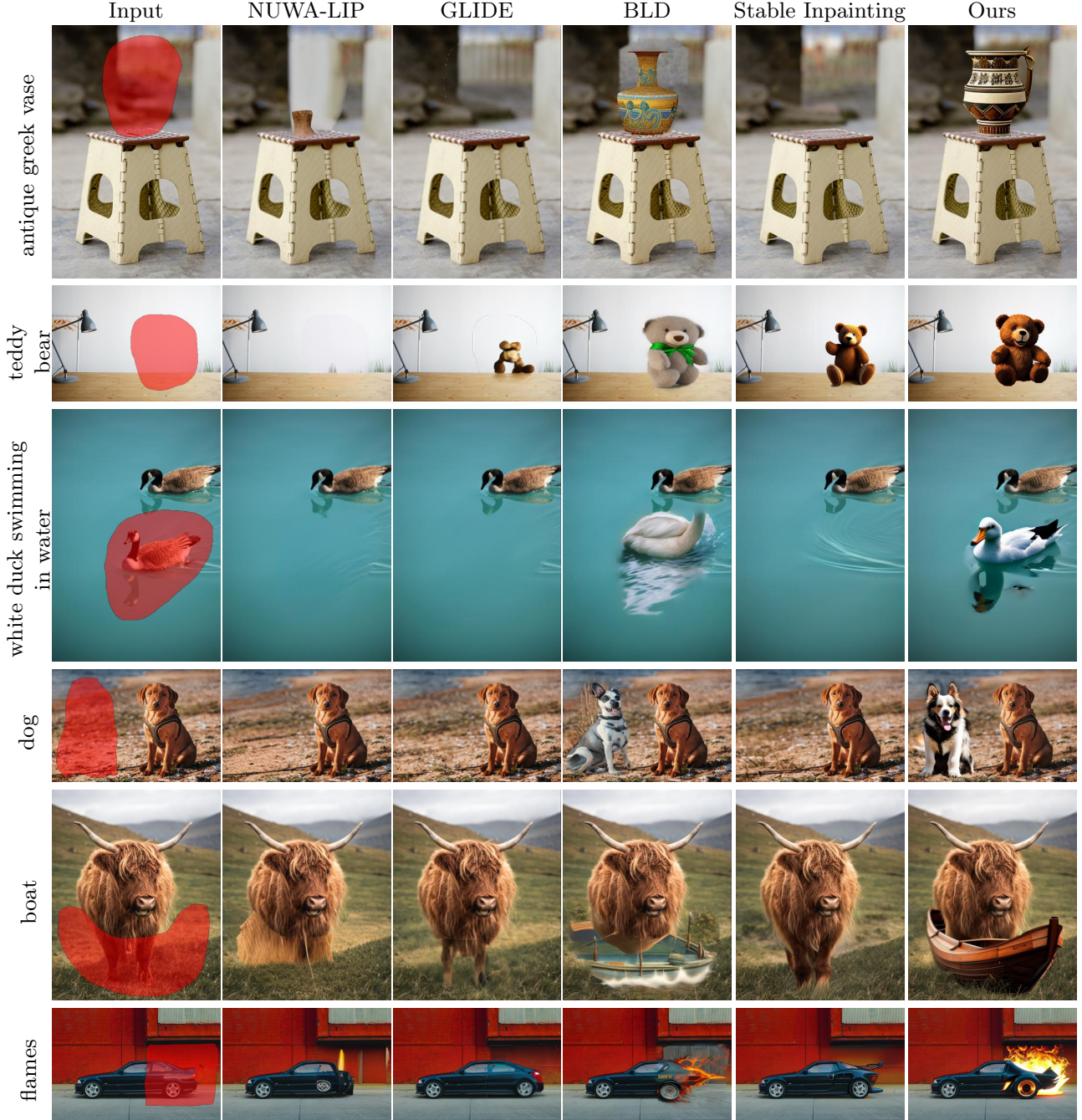


Figure 4. Comparison with state-of-the-art text-guided inpainting methods. Zoom in for details. For more comparison see Appendix.

quantitatively. We also provide more discussion on each of them in our supplementary material, including thorough analyses on their impact, demonstrated by visuals.

5. Conclusion

In this paper, we introduced a training-free approach to text-guided high-resolution image inpainting, addressing the prevalent challenges of prompt neglect: background and nearby object dominance. Our contributions, the

Prompt-Aware Introverted Attention (PAIntA) layer and the Reweighting Attention Score Guidance (RASG) mechanism, effectively mitigate the mentioned issues leading our method to surpass the existing state-of-the-art approaches qualitatively and quantitatively. Additionally, our unique inpainting-specific super-resolution technique offers seamless completion in high-resolution images, distinguishing our method from existing solutions.

References

- [1] Omri Avrahami, Dani Lischinski, and Ohad Fried. Blended diffusion for text-driven editing of natural images. In *Proceedings of the IEEE/CVF Conference on Computer Vision and Pattern Recognition*, pages 18208–18218, 2022.
- [2] Omri Avrahami, Ohad Fried, and Dani Lischinski. Blended latent diffusion. *ACM Transactions on Graphics (TOG)*, 42(4):1–11, 2023.
- [3] Tim Brooks, Aleksander Holynski, and Alexei A Efros. Instructpix2pix: Learning to follow image editing instructions. In *Proceedings of the IEEE/CVF Conference on Computer Vision and Pattern Recognition*, pages 18392–18402, 2023.
- [4] Hila Chefer, Yuval Alaluf, Yael Vinker, Lior Wolf, and Daniel Cohen-Or. Attend-and-excite: Attention-based semantic guidance for text-to-image diffusion models. *ACM Transactions on Graphics (TOG)*, 42(4):1–10, 2023.
- [5] K Chen, J Wang, J Pang, Y Cao, Y Xiong, X Li, S Sun, W Feng, Z Liu, J Xu, et al. Mmdetection: Open mmlab detection toolbox and benchmark. arxiv 2019. *arXiv preprint arXiv:1906.07155*, 2019.
- [6] Prafulla Dhariwal and Alexander Nichol. Diffusion models beat gans on image synthesis. *Advances in neural information processing systems*, 34:8780–8794, 2021.
- [7] Dave Epstein, Allan Jabri, Ben Poole, Alexei A Efros, and Aleksander Holynski. Diffusion self-guidance for controllable image generation. *arXiv preprint arXiv:2306.00986*, 2023.
- [8] Patrick Esser, Robin Rombach, and Bjorn Ommer. Taming transformers for high-resolution image synthesis. In *Proceedings of the IEEE/CVF conference on computer vision and pattern recognition*, pages 12873–12883, 2021.
- [9] Rinon Gal, Yuval Alaluf, Yuval Atzmon, Or Patashnik, Amit H Bermano, Gal Chechik, and Daniel Cohen-Or. An image is worth one word: Personalizing text-to-image generation using textual inversion. *arXiv preprint arXiv:2208.01618*, 2022.
- [10] Vedit Goel, Elia Peruzzo, Yifan Jiang, Dejia Xu, Nicu Sebe, Trevor Darrell, Zhangyang Wang, and Humphrey Shi. Pair-diffusion: Object-level image editing with structure-and-appearance paired diffusion models. *arXiv preprint arXiv:2303.17546*, 2023.
- [11] Amir Hertz, Ron Mokady, Jay Tenenbaum, Kfir Aberman, Yael Pritch, and Daniel Cohen-Or. Prompt-to-prompt image editing with cross attention control. *arXiv preprint arXiv:2208.01626*, 2022.
- [12] Jonathan Ho, Ajay Jain, and Pieter Abbeel. Denoising diffusion probabilistic models. *Advances in neural information processing systems*, 33:6840–6851, 2020.
- [13] Itseez. Open source computer vision library. <https://github.com/itseez/opencv>, 2015.
- [14] Tero Karras, Samuli Laine, Miika Aittala, Janne Hellsten, Jaakko Lehtinen, and Timo Aila. Analyzing and improving the image quality of stylegan. In *Proceedings of the IEEE/CVF conference on computer vision and pattern recognition*, pages 8110–8119, 2020.
- [15] Yuval Kirstain, Adam Polyak, Uriel Singer, Shahbuland Matiana, Joe Penna, and Omer Levy. Pick-a-pic: An open dataset of user preferences for text-to-image generation. *arXiv preprint arXiv:2305.01569*, 2023.
- [16] Tsung-Yi Lin, Michael Maire, Serge Belongie, James Hays, Pietro Perona, Deva Ramanan, Piotr Dollár, and C Lawrence Zitnick. Microsoft coco: Common objects in context. In *Computer Vision–ECCV 2014: 13th European Conference, Zurich, Switzerland, September 6–12, 2014, Proceedings, Part V 13*, pages 740–755. Springer, 2014.
- [17] Guilin Liu, Fitsum A Reda, Kevin J Shih, Ting-Chun Wang, Andrew Tao, and Bryan Catanzaro. Image inpainting for irregular holes using partial convolutions. In *Proceedings of the European conference on computer vision (ECCV)*, pages 85–100, 2018.
- [18] Haoming Lu, Hazarpet Tunanyan, Kai Wang, Shant Navasardyan, Zhangyang Wang, and Humphrey Shi. Specialist diffusion: Plug-and-play sample-efficient fine-tuning of text-to-image diffusion models to learn any unseen style. In *Proceedings of the IEEE/CVF Conference on Computer Vision and Pattern Recognition*, pages 14267–14276, 2023.
- [19] Chong Mou, Xintao Wang, Liangbin Xie, Jian Zhang, Zhonggang Qi, Ying Shan, and Xiaohe Qie. T2i-adapter: Learning adapters to dig out more controllable ability for text-to-image diffusion models. *arXiv preprint arXiv:2302.08453*, 2023.
- [20] Shant Navasardyan and Marianna Ohanyan. Image inpainting with onion convolutions. In *proceedings of the asian conference on computer vision*, 2020.
- [21] Minheng Ni, Xiaoming Li, and Wangmeng Zuo. Nuwa-lip: Language-guided image inpainting with defect-free vqgan. In *Proceedings of the IEEE/CVF Conference on Computer Vision and Pattern Recognition*, pages 14183–14192, 2023.
- [22] Alex Nichol, Prafulla Dhariwal, Aditya Ramesh, Pranav Shyam, Pamela Mishkin, Bob McGrew, Ilya Sutskever, and Mark Chen. Glide: Towards photorealistic image generation and editing with text-guided diffusion models. *arXiv preprint arXiv:2112.10741*, 2021.
- [23] Patrick Pérez, Michel Gangnet, and Andrew Blake. *Poisson Image Editing*. Association for Computing Machinery, New York, NY, USA, 1 edition, 2023.
- [24] John David Pressman, Katherine Crowson, and Simulacra Captions Contributors. Simulacra aesthetic captions. Technical Report Version 1.0, Stability AI, 2022. url <https://github.com/JD-P/simulacra-aesthetic-captions>.
- [25] Alec Radford, Jong Wook Kim, Chris Hallacy, Aditya Ramesh, Gabriel Goh, Sandhini Agarwal, Girish Sastry, Amanda Askell, Pamela Mishkin, Jack Clark, et al. Learning transferable visual models from natural language supervision. In *International conference on machine learning*, pages 8748–8763. PMLR, 2021.
- [26] Aditya Ramesh, Prafulla Dhariwal, Alex Nichol, Casey Chu, and Mark Chen. Hierarchical text-conditional image generation with clip latents. *arXiv preprint arXiv:2204.06125*, 1(2):3, 2022.
- [27] Robin Rombach, Andreas Blattmann, Dominik Lorenz, Patrick Esser, and Björn Ommer. High-resolution image synthesis with latent diffusion models. In *Proceedings of the IEEE/CVF conference on computer vision and pattern recognition*, pages 10684–10695, 2022.

- [28] Olaf Ronneberger, Philipp Fischer, and Thomas Brox. U-net: Convolutional networks for biomedical image segmentation. In *Medical Image Computing and Computer-Assisted Intervention–MICCAI 2015: 18th International Conference, Munich, Germany, October 5–9, 2015, Proceedings, Part III* 18, pages 234–241. Springer, 2015.
- [29] Nataniel Ruiz, Yuanzhen Li, Varun Jampani, Yael Pritch, Michael Rubinstein, and Kfir Aberman. Dreambooth: Fine tuning text-to-image diffusion models for subject-driven generation. In *Proceedings of the IEEE/CVF Conference on Computer Vision and Pattern Recognition*, pages 22500–22510, 2023.
- [30] Chitwan Saharia, William Chan, Saurabh Saxena, Lala Li, Jay Whang, Emily L Denton, Kamyar Ghasemipour, Raphael Gontijo Lopes, Burcu Karagol Ayan, Tim Salimans, et al. Photorealistic text-to-image diffusion models with deep language understanding. *Advances in Neural Information Processing Systems*, 35:36479–36494, 2022.
- [31] Andranik Sargsyan, Shant Navasardyan, Xingqian Xu, and Humphrey Shi. Mi-gan: A simple baseline for image inpainting on mobile devices. In *Proceedings of the IEEE/CVF International Conference on Computer Vision (ICCV)*, pages 7335–7345, 2023.
- [32] Christoph Schuhmann, Romain Beaumont, Richard Vencu, Cade Gordon, Ross Wightman, Mehdi Cherti, Theo Coombes, Aarush Katta, Clayton Mullis, Mitchell Wortsman, et al. Laion-5b: An open large-scale dataset for training next generation image-text models. *Advances in Neural Information Processing Systems*, 35:25278–25294, 2022.
- [33] Jascha Sohl-Dickstein, Eric Weiss, Niru Maheswaranathan, and Surya Ganguli. Deep unsupervised learning using nonequilibrium thermodynamics. In *International conference on machine learning*, pages 2256–2265. PMLR, 2015.
- [34] Jiaming Song, Chenlin Meng, and Stefano Ermon. Denoising diffusion implicit models. In *International Conference on Learning Representations*, 2021.
- [35] Aaron Van Den Oord, Oriol Vinyals, et al. Neural discrete representation learning. *Advances in neural information processing systems*, 30, 2017.
- [36] Su Wang, Chitwan Saharia, Ceslee Montgomery, Jordi Pont-Tuset, Shai Noy, Stefano Pellegrini, Yasumasa Onoe, Sarah Laszlo, David J Fleet, Radu Soricut, et al. Imagen editor and editbench: Advancing and evaluating text-guided image inpainting. In *Proceedings of the IEEE/CVF Conference on Computer Vision and Pattern Recognition*, pages 18359–18369, 2023.
- [37] Chenfei Wu, Jian Liang, Lei Ji, Fan Yang, Yuejian Fang, Daxin Jiang, and Nan Duan. Nüwa: Visual synthesis pre-training for neural visual world creation. In *European conference on computer vision*, pages 720–736. Springer, 2022.
- [38] Shaoan Xie, Zhifei Zhang, Zhe Lin, Tobias Hinz, and Kun Zhang. Smartbrush: Text and shape guided object inpainting with diffusion model. In *Proceedings of the IEEE/CVF Conference on Computer Vision and Pattern Recognition*, pages 22428–22437, 2023.
- [39] Xingqian Xu, Jiayi Guo, Zhangyang Wang, Gao Huang, Irfan Essa, and Humphrey Shi. Prompt-free diffusion: Taking “text” out of text-to-image diffusion models. *arXiv preprint arXiv:2305.16223*, 2023.
- [40] Xingqian Xu, Shant Navasardyan, Vahram Tadevosyan, Andranik Sargsyan, Yadong Mu, and Humphrey Shi. Image completion with heterogeneously filtered spectral hints. In *Proceedings of the IEEE/CVF Winter Conference on Applications of Computer Vision*, pages 4591–4601, 2023.
- [41] Xingqian Xu, Zhangyang Wang, Gong Zhang, Kai Wang, and Humphrey Shi. Versatile diffusion: Text, images and variations all in one diffusion model. In *Proceedings of the IEEE/CVF International Conference on Computer Vision*, pages 7754–7765, 2023.
- [42] Zili Yi, Qiang Tang, Shekoofeh Azizi, Daesik Jang, and Zhan Xu. Contextual residual aggregation for ultra high-resolution image inpainting. In *Proceedings of the IEEE/CVF conference on computer vision and pattern recognition*, pages 7508–7517, 2020.
- [43] Jiahui Yu, Zhe Lin, Jimei Yang, Xiaohui Shen, Xin Lu, and Thomas S Huang. Generative image inpainting with contextual attention. In *Proceedings of the IEEE conference on computer vision and pattern recognition*, pages 5505–5514, 2018.
- [44] Jiahui Yu, Zhe Lin, Jimei Yang, Xiaohui Shen, Xin Lu, and Thomas S Huang. Free-form image inpainting with gated convolution. In *Proceedings of the IEEE/CVF international conference on computer vision*, pages 4471–4480, 2019.
- [45] Lvmin Zhang and Maneesh Agrawala. Adding conditional control to text-to-image diffusion models. *arXiv preprint arXiv:2302.05543*, 2023.
- [46] Shengyu Zhao, Jonathan Cui, Yilun Sheng, Yue Dong, Xiao Liang, Eric I Chang, and Yan Xu. Large scale image completion via co-modulated generative adversarial networks. *arXiv preprint arXiv:2103.10428*, 2021.
- [47] Haitian Zheng, Zhe Lin, Jingwan Lu, Scott Cohen, Eli Shechtman, Connelly Barnes, Jianming Zhang, Ning Xu, Sohrab Amirghodsi, and Jiebo Luo. Cm-gan: Image inpainting with cascaded modulation gan and object-aware training. *arXiv preprint arXiv:2203.11947*, 2022.

Appendix A. Additional Quantitative Comparison and Ablation

Most real-world applications of Stable-Diffusion based models often use sets of generic positive and negative prompts to enhance the visual fidelity of the generated objects/scenes (e.g. "High quality", "HD", "Realistic", etc as positive, and "Blurred", "Low Quality", "Out of frame" etc. as negative). In this section we provide an additional quantitative comparison that utilizes generic quality-enhancing positive/negative prompts for the methods that benefit from them. We have used the following standard set of positive/negative words for all our samples:

Positive prompt: *Full HD, 4K, high quality, high resolution*

Negative prompt: *text, bad anatomy, bad proportions, blurry, cropped, deformed, disfigured, duplicate, error, extra limbs, gross proportions, jpeg artifacts, long neck, low quality, lowres, malformed, morbid, mutated, mutilated, out of frame, ugly, worst quality*

In Tab. 3 we present an additional evaluation of our method and its ablations with the subset of the competitors that work with positive/negative prompts. To measure the visual fidelity of the results we additionally employ the LAION aesthetic score². The aesthetic score is computed by an MLP trained on 5000 image-rating pairs from the Simulacra Aesthetic Captions dataset [24], and can be used to assign a value from the [0, 10] range to images based on their aesthetic appeal.

As can be seen from that table the positive/negative prompts not only have a positive effect on the visual quality of the images (as seen from the improvement of the aesthetic score), but also positively affect the accuracy of our methods. However, due to the slight drop in the CLIP Score, using these prompts can be seen as a trade-off based one whether CLIP Score or accuracy / aesthetic score are valued more.

	w/o Pos./Neg.			with Pos./Neg.		
Model Name	CLIP ↑	Acc ↑	Aes. ↑	CLIP ↑	Acc ↑	Aes. ↑
GLIDE	24.92	44.0 %	4.475	25.02	42.5 %	4.488
BLD	24.82	49.8 %	4.808	25.06	53.0 %	4.951
Stable-Inp.	24.87	51.9 %	4.878	24.89	56.8 %	5.005
(only PAIntA)	25.24	52.2 %	4.861	25.36	60.9 %	5.013
(only RASG)	25.85	62.0 %	4.872	25.32	62.0 %	5.008
RASG & PAIntA	26.34	61.4 %	4.843	25.65	65.0 %	5.021

Table 3. Quantitative comparison with and without using positive/negative prompts during generation for all models

²<https://github.com/christophschuhmann/improved-aesthetic-predictor>

Appendix B. Extended Qualitative Comparison

Here in Fig. 16 we show more visual comparison with the other state-of-the-art methods. Fig. 17 includes more comparison on the validation set of MSCOCO 2017 [16]. The results show the advantage of our method over the baselines.

In Fig. 13 we compare our inpainting-specialized super-resolution method with vanilla approaches of Bicubic or Stable Super-Resolution-based upscaling of the inpainting results followed by Poisson blending in the unknown region. We can clearly see that our method, leveraging the known region fine-grained information, can seamlessly fill in with high quality. In Figures 18 and 19 we show more visual comparison between our method and the approach of Stable Super-Resolution.

Appendix C. Robustness to the Random Seed

Since diffusion-based models generate output images by denoising a randomly sampled starting noise, the resulting outputs are stochastic, and depend on the sampled starting noise. To verify that the insights formulated during the visual comparison with the baselines are consistent, and are not a mere consequence of random chance, we repeated several generations for five randomly sampled starting seeds. In Fig. 21, 22 and 23 we show the results for five different seeds. As can be noticed our method is able to generate the prompt-aligned objects regardless the initial noise, whereas the competitors perform the desired generation not so frequently.

Appendix D. User Study

In addition to the qualitative/quantitative comparisons with the existing state-of-the-art approaches, we also performed a user study. We included 10 people in the study who were asked to assess 5 text-guided inpainting methods: NUWA-LIP [21], GLIDE [22], BLD [2], Stable Inpainting [27], and Ours. The participants were provided with 20 (*image, mask, prompt*) triplets and the inpainting results of the 5 methods in the random order, and for each image were asked the following questions:

- Which results best match user prompt?
- Which results have the best overall quality (considering both prompt alignment and image quality)?

The participants were allowed to choose none or multiple best methods since some approaches can perform equally good or all of them be equally bad. After collecting the feedback from the users we calculate the total votes for all the methods and for both questions. The results are presented in Fig. 5 demonstrating a clear advantage of our method in both aspects: prompt alignment and overall quality.

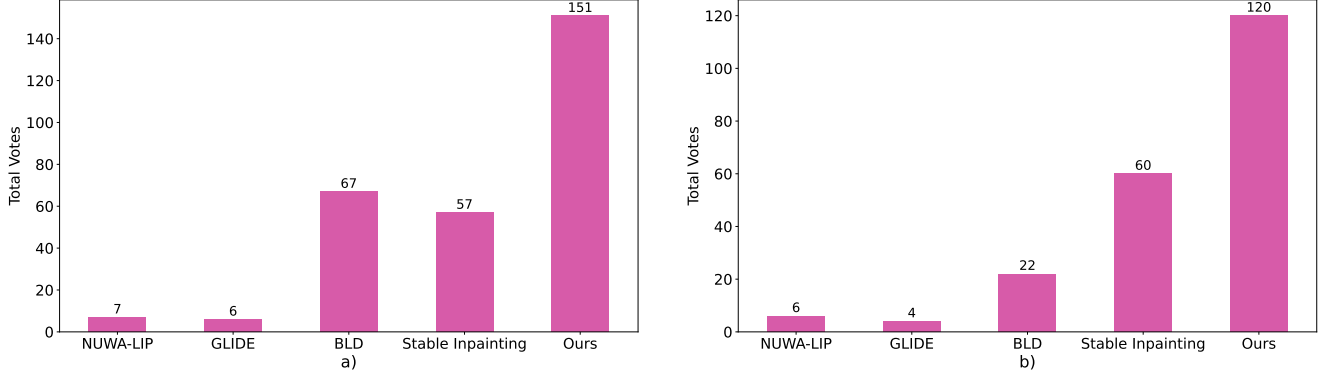


Figure 5. Total votes of each method based on our user study for questions a) *Which results best match user prompt?* and b) *Which results have the best overall quality (considering both prompt alignment and image quality)?* The user study shows a clear advantage of our method.

Appendix E. Discussion on PAIntA

In this section we discuss the effectiveness of the proposed PAIntA module as a plug-in replacement for self-attention (SA) layers. To that end, first we visualize SA similarity maps averaged across masked locations from resolutions $H/16 \times W/16$ and $H/32 \times W/32$ where PAIntA is applied (see Fig. 6). Then, we see that PAIntA successfully scales down the similarities of masked locations with prompt-unrelated locations from the known region, and, as a result, a prompt-specified object is generated inside the mask.

For a given resolution ($H/16 \times W/16$ or $H/32 \times W/32$), in order to visualize the average SA similarity map across masked pixels, first we resize the input mask to match the dimensions of the corresponding resolution (we use nearest interpolation in resize operation). Then, for each SA layer in the given resolution, we form a 2D similarity map by reshaping and averaging the similarity matrix rows corresponding to the masked region. Further, we average obtained 2D similarity maps across all SA layers (of the given resolution) and diffusion timesteps. More specifically, if $A_{self}^1, \dots, A_{self}^L \in \mathbb{R}^{h \times w}$ ($h \times w$ is either $H/16 \times W/16$ or $H/32 \times W/32$) are the self-attention matrices of Stable Inpainting layers of the given resolution, and, respectively, are being updated by PAIntA to the matrices \tilde{A}_{self}^i (see Eq. 5), then we consider the following similarity maps:

$$A = \frac{1}{|M| \cdot L} \sum_{i, M_i=1} \sum_{l=1}^L (A_{self}^l)_i \in \mathbb{R}^{h \times w},$$

$$\tilde{A} = \frac{1}{|M| \cdot L} \sum_{i, M_i=1} \sum_{l=1}^L (\tilde{A}_{self}^l)_i \in \mathbb{R}^{h \times w},$$

and reshape them to 2D matrices of size $h \times w$. So, A_{ij} and \tilde{A}_{ij} show the average amount in which masked pixels attend to other locations in the cases of the vanilla self-attention

and PAIntA respectively. Finally, in order to visualize the similarity maps, we use bicubic resize operation to match it with the image dimensions and plot the similarity heatmap using JET colormap from OpenCV [13].

Next, we compare the generation results and corresponding similarity maps obtained from above procedure when PAIntA’s SA scaling is (the case of \tilde{A}) or is not (the case of A) used. Because PAIntA’s scaling is only applied on $H/32 \times W/32$ and $H/16 \times W/16$ resolutions, we are interested in those similarity maps. Rows 1-3 in Fig. 6 demonstrate visualizations on *nearby object dominance* issue (when known objects are continued to the inpainted region while ignoring the prompt) of the vanilla diffusion inpainting, while rows 4-6 demonstrate those of with *background dominance* issue (when nothing is generated, just the background is coherently filled in).

For example, on row 1, Fig. 6 in case of *Stable Inpainting without PAIntA* generation, the average similarity of the masked region is dominated by the known regions of the car on both 16 and 32 resolutions. Whereas, as a result of PAIntA scaling application, the average similarity of the masked region with the car is effectively reduced, and the masked region is generated in accordance to the input prompt.

Row 4, Fig. 6 demonstrates an example where known region contains a dog, which is aligned with the input prompt. In this case, visualization shows that PAIntA successfully reduces the similarity of the masked region with the unrelated background while preserving the similarity with the dog. This example too shows that by reducing the similarity of masked region with the unrelated known regions PAIntA enables prompt-faithful generation. You can find additional examples of PAIntA’s effect on the final generation in Fig. 7.

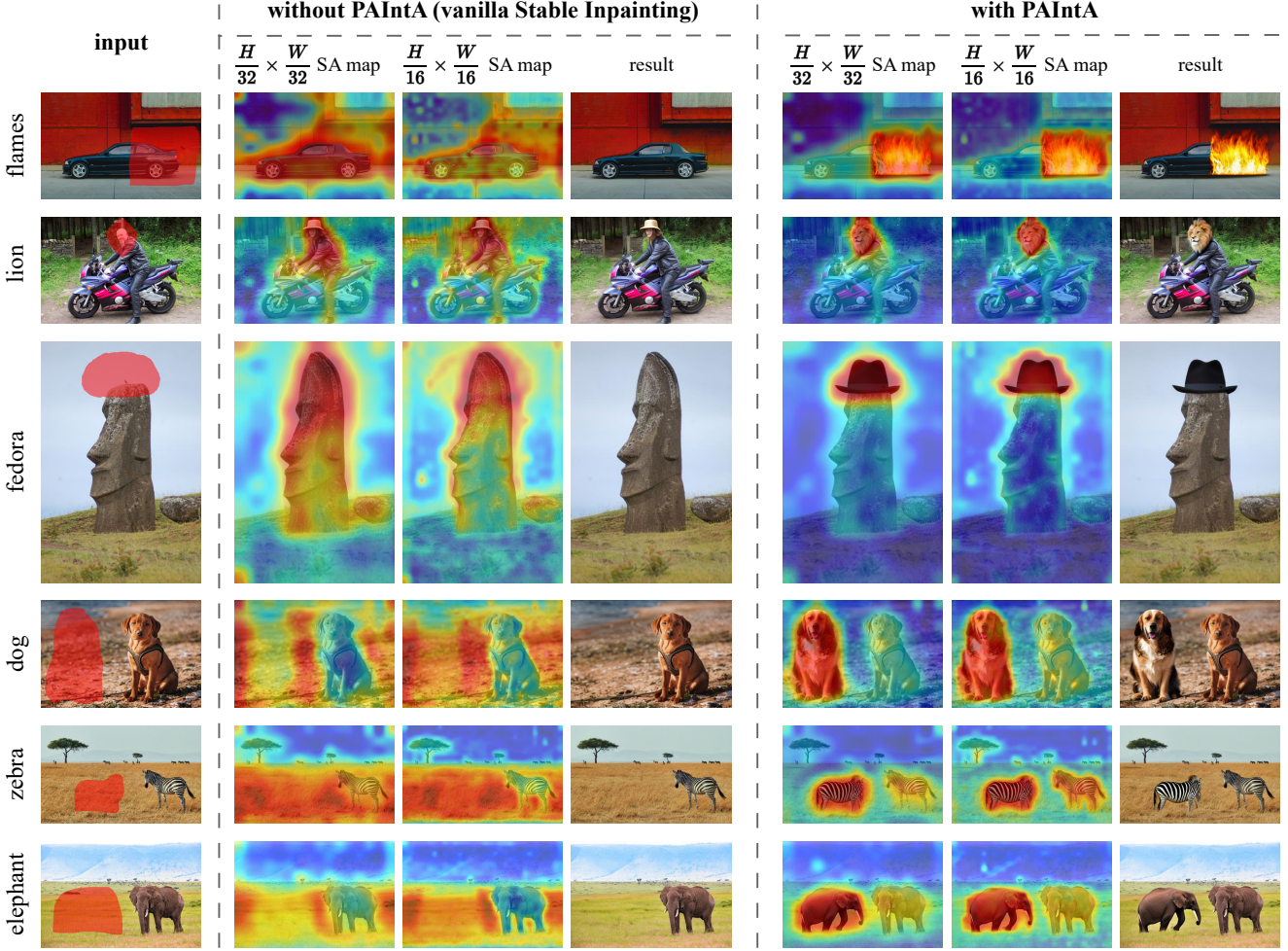


Figure 6. Comparison of self-attention similarity maps averaged across masked pixels for generations without/with PAIntA’s scaling of the original self-attention scores. Images are generated from the same seed.

Appendix F. Discussion on RASG

In this section we discuss the choice of RASG objective guidance function $S(x)$, then demonstrate the effect of RASG and motivate the part of gradient reweighting by its standard deviation. Finally, we present additional examples of RASG’s effect on the final generation in Fig. 8.

Appendix F.1. The Objective Function $S(x)$

As we already mentioned in the main paper, Stable Inpainting may fail to generate certain objects in the prompt, completely neglecting them in the process. We categorized these cases into two types, namely background and nearby object dominance issues. [4] also mentions these issues but for text-to-image generation task, and refers them as *catastrophic neglect* problem. To alleviate this problem [4] propose a mechanism called *generative semantic nursing*, allowing the users to “boost” certain tokens in the prompt,

ensuring their generation. In essence the mechanism is a post-hoc guidance with a chosen objective function maximizing the maximal cross-attention score of the image with the token which should be “boosted”. This approach can be easily adapted to the inpainting task by just restricting the maximum to be taken in an unknown region so that the object is generated there, and averaging the objectives across all tokens, since we don’t have specific tokens to “boost”, but rather care about all of them. In other words, by our notations from the main paper, the following guidance objective function can be used:

$$S(x_t) = -\frac{1}{|ind(\tau)|} \sum_{k \in ind(\tau)} \max_{i: M_i=1} \{\bar{A}^k(x_t)_i\}. \quad (11)$$

However we noticed that with this approach the shapes/sizes of generated objects might not be sufficiently aligned with the shape/size of the input mask, which is often desirable for text-guided inpainting (see Fig.



Figure 7. Visual ablation of PAIntA. Generated images use the same seed. In row 3 only PAIntA is used.

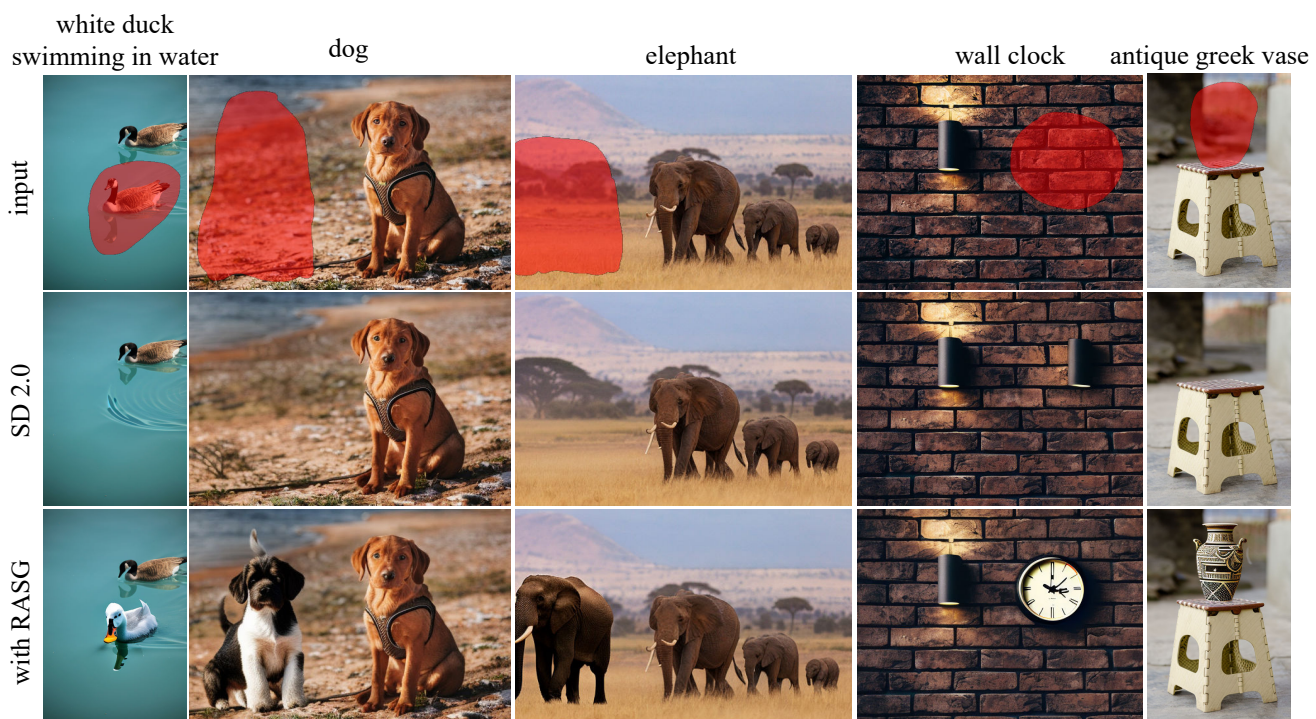


Figure 8. Visual ablation of RASG. Generated images use the same seed. In row 3 only RASG is used.

12). Therefore, we utilize the segmentation property of cross-attention similarity maps, by so using *Binary Cross*

Entropy as the energy function for guidance (see Eq. 9 in the main paper). As can be noticed from Fig. 12 the results

with the binary cross-entropy better fit the shape of the inpainting mask.

Appendix F.2. Effect of RASG Strategy

Although the objective function $S(x)$ defined by Eq. 9 (main paper) results in better mask shape/size aligned inpainting, the vanilla post-hoc guidance may lead the latents to become out of their trained domain as also noted by [4]: “many updates of x_t may lead to the latent becoming out-of-distribution, resulting in incoherent images”. Due to this the post-hoc guidance mechanism (semantic nursing) by [4] is done using multiple iterations of very small, iterative perturbations of x_t , which makes the process considerably slow. In addition, the generation can still fail if the iterative process exceeds the maximum iteration limit without reaching the necessary thresholds.

Thanks to RASG’s seamless integration of the $\nabla_{x_t} S(x_t)$ gradient component into the general form of DDIM diffusion sampling, our RASG mechanism keeps the modified latents x_t within the expected distribution, while introducing large enough perturbations to x_t with only one iteration of guidance per time-step. This allows to generate the objects described in the prompts coherently with the known region without extra-cost of time.

Fig. 9 demonstrates the advantage of RASG’s strategy over the vanilla guidance mechanism. Indeed, in the vanilla post-hoc guidance there is a hyperparameter s controlling the amount of guidance. When s is too small (e.g. close to 0 or for some cases $s = 100$) the vanilla guidance mechanism does not show much effect due to too small guidance from $s\nabla_{x_t} S(x_t)$. Then with increasing the hyperparameter ($s = 1000, 10000$) one can notice more and more text/shape alignment with prompt/inpainting mask, however the generated results are unnatural and incoherent with the known region. This is made particularly challenging by the fact, that different images, or even different starting seeds with the same input image might require different values of the perturbation strength to achieve the best result. In contrast, RASG approach is *hyperparameter-free* allowing both: prompt/mask-aligned and naturally looking results.

Appendix F.3. Rescaling with Standard Deviation

The core idea of RASG is to automatically scale perturbation using certain heuristics, such that the guidance process has a consistent effect on the output, without harming the quality of the image. Our main heuristic relies on the fact that [34] have defined a parametric family of stochastic denoising processes, which can all be trained using the same training objective as DDPM [12]. Recall the general form

of parametric family of DDIM sampling processes:

$$x_{t-1} = \sqrt{\alpha_{t-1}} \frac{x_t - \sqrt{1 - \alpha_t} \epsilon_\theta^t(x_t)}{\sqrt{\alpha_t}} + \sqrt{1 - \alpha_{t-1} - \sigma_t^2 \epsilon_\theta^t(x_t) + \sigma_t \epsilon_t}, \quad (12)$$

where $\epsilon_t \sim \mathcal{N}(\mathbf{0}, \mathbf{1})$. Particularly ϵ_t can be taken to be collinear with the gradient $\nabla_{x_t} S(x_t)$ which will result in x_{t-1} distribution preservation by at the same time guiding the generation process towards minimization of $S(x_t)$.

Therefore we propose to scale the gradient $\nabla_{x_t} S(x_t)$ with a value λ and use instead of ϵ_t in the general form of DDIM. To determine λ we analyse the distribution of $\nabla_{x_t} S(x_t)$ and found out that the values of the gradients have a distribution very close to a gaussian distribution, with 0 mean and some arbitrary σ , which changes over time-step/image (Fig. 10). Therefore, computing the standard deviation of the values of $\nabla_{x_t} S(x_t)$, and normalizing it by $\lambda = \frac{1}{std(\nabla_{x_t} S(x_t))}$ results in the standard normal distribution (see Fig. 11). So the final form of RASG guidance strategy is

$$x_{t-1} = \sqrt{\alpha_{t-1}} \frac{x_t - \sqrt{1 - \alpha_t} \epsilon_\theta^t(x_t)}{\sqrt{\alpha_t}} + \sqrt{1 - \alpha_{t-1} - \sigma_t^2 \epsilon_\theta^t(x_t) + \sigma_t \frac{\nabla_{x_t} S(x_t)}{std(\nabla_{x_t} S(x_t))}}. \quad (13)$$

Appendix G. Visual Examples For Ablation Study

In Fig. 24 we show that RASG and PAIntA are crucial parts of our method. It’s worth noting that for example in the cases when another instance of the prompt object is present in the known region (e.g. in the first row of Fig. 24 another zebra is present in the known part) PAIntA is still able to generate the desired object. This is thanks to its ability to enhance the impact of such known region pixels that are more aligned with the given prompt (zebra pixels in the known region will have high similarity to the prompt “zebra” resulting in high values of c_j).

However sometimes, especially in the case of *background dominance* issue, the PAIntA’s ability to reduce the impact of the background non-prompt-related pixels is not enough (it does not allow the background to dominate through the attention scores, but also has no mechanism to directly force the inpainted region align the prompt), and, in such situations, RASG is helping to directly maximize the prompt-generation alignment in the missing region. Similarly, sometimes if only RASG applied, the background dominance can be so strong that RASG’s direct guidance may be not enough for proper generation of the objects mentioned in the prompt. By so we conclude that the contributions of PAIntA and RASG are perpendicular and work best when applied together.

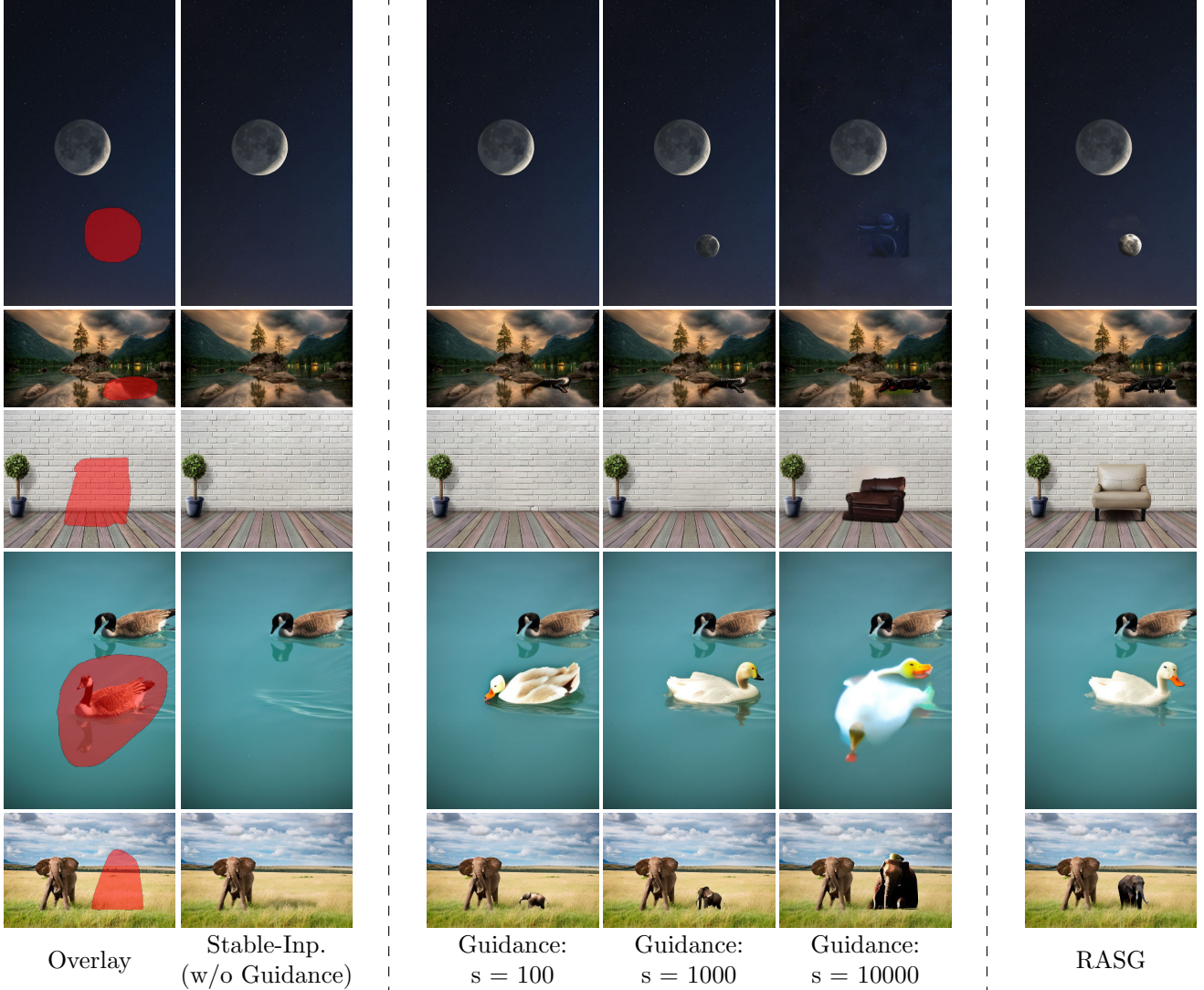


Figure 9. Comparison of RASG strategy with default Stable Inpainting and vanilla guidance mechanism with different guidance scales. In contrast to vanilla guidance, where the generation highly depends on the guidance scale, RASG consistently produces naturally looking and prompt-aligned results.

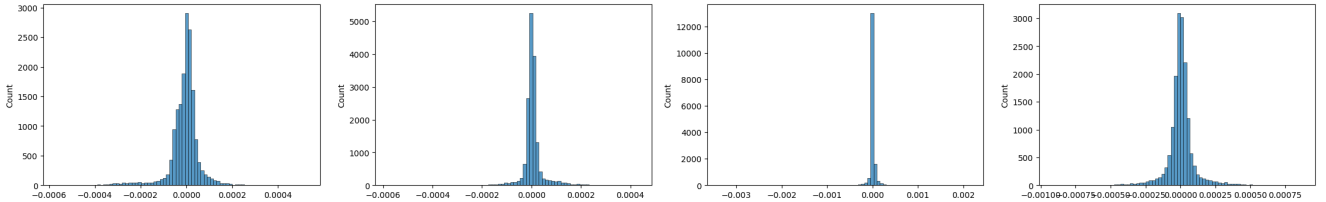


Figure 10. Histogram of $\nabla_{x_t} S(x_t)$ values (i.e. before gradient standardization)

Appendix H. Generation Of Existing Objects

We noticed from Fig. 4 (main paper) that the competitor methods frequently fail to generate objects when the input image already contains an object of the same type. To verify

that the failure is caused by the existence of the object, we first removed the existing object from the original and fill it in with background. For that we use the Stable Inpainting method, by providing an empty prompt. We then evaluate the competitor methods on the modified image with the

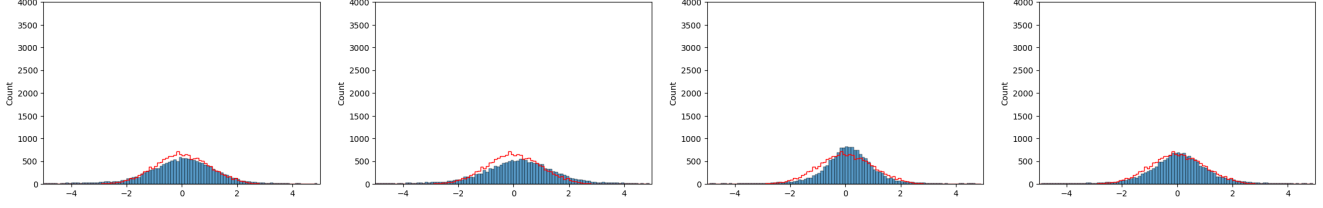


Figure 11. Histogram of $\frac{\nabla_{x_t} S(x_t)}{\text{std}(\nabla_{x_t} S(x_t))}$ values (i.e. after gradient standardization)

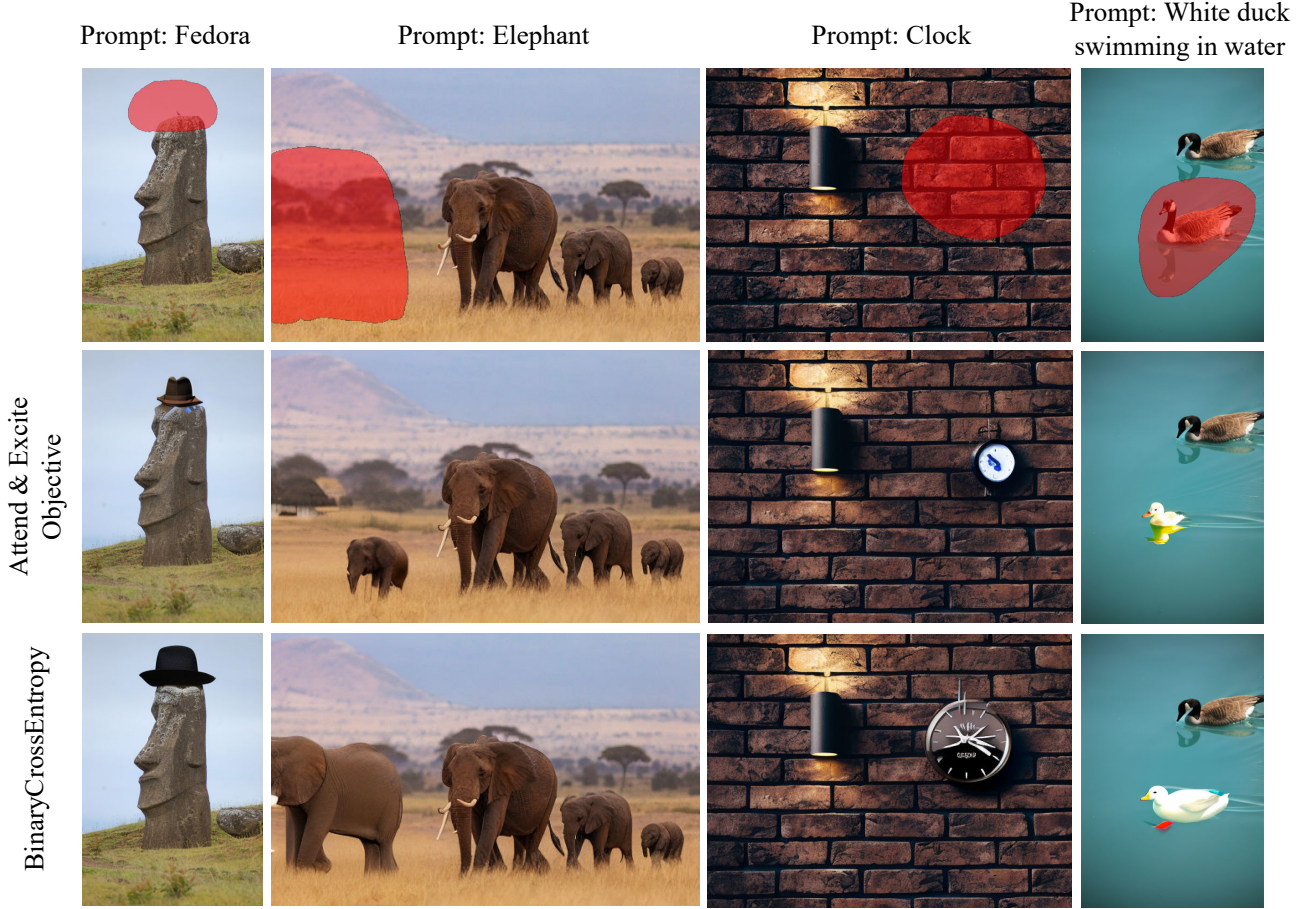


Figure 12. Comparison of the Binary Cross Entropy engery function to modified version of Attend & Excite. Images generated from the same seed.

original masks and prompts. As can be seen in Fig. 20, the models are in fact able to generate the corresponding objects in this case. We hypothesize that the reason of not generating the object when another instance of the same class is present is that cross-attention layers are designed to just ensure the presence of prompt objects without forcing them to be generated in a specific location indicated by the inpainting mask. In contrast with this our PAIntA layer forces the sampling process to pay more attention on the unknown region alignment with the prompt.

Appendix I. More Examples of Our Method

We present more results of our method both for low-resolution (512 for the long side) images (Fig. 25), as well as high-resoluition (2048 for the long side) (Figures 26, 27, 28).

Appendix J. Limitations

Although our method improves the prompt-alignment of existing text-guided inpainting approaches, it still has a depen-

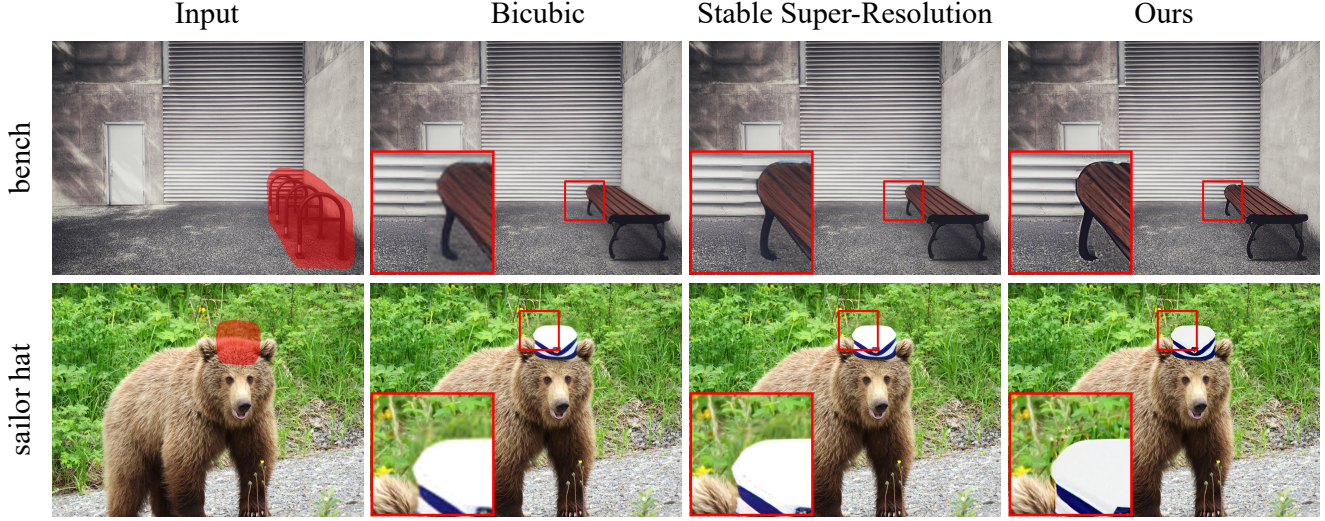


Figure 13. Comparison of our inpainting-specialized super-resolution approach with vanilla upscaling methods for inpainting. Best viewed when zoomed in.



Figure 14. Failure examples produced by our approach.

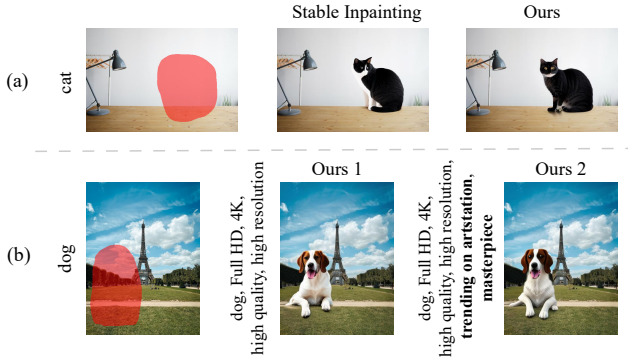


Figure 15. Sources of unnatural generation issues in our approach. (a) Unnatural generation case when the issue comes from the base model itself. (b) Example showing the sensitivity of our approach to carelessly chosen positive words. Left result is generated using only neutral positive words. Right result is generated using additional, non-aligned positive words causing generation to be less natural.

dency on the backbone model, hence inherits some quality limitations. Particularly it may generate extra limbs (the elephant in Fig. 14 has 5 legs) or illogical appearances (the sheep appears to have two bodies in Fig. 14 after the inpainting).

Besides illogical issues, our method can sometimes pro-

duce unnatural results. First of all, unnatural results can be attributed to the underlying base model, which in our case is Stable Inpainting (e.g. see Fig. 15.a). Furthermore, sometimes our approach, due to its prompt-faithfulness, may become over-sensitive to positive/negative words which may lead to unnatural results when those are not carefully picked. For example, as can be seen in Fig. 15.b, the addition of positive words *trending on artstation* and *masterpiece*, which usually appear in the context of artistic images, causes the generated dog to become considerably less natural as opposed to the generation with only neutral positive prompts. This happens, because our method limits the use of prompt-unrelated visual context, and guides the generation towards the user provided prompt, so that in case prompt contains unrelated positive tokens, the generated content may be shifted from the visual context.

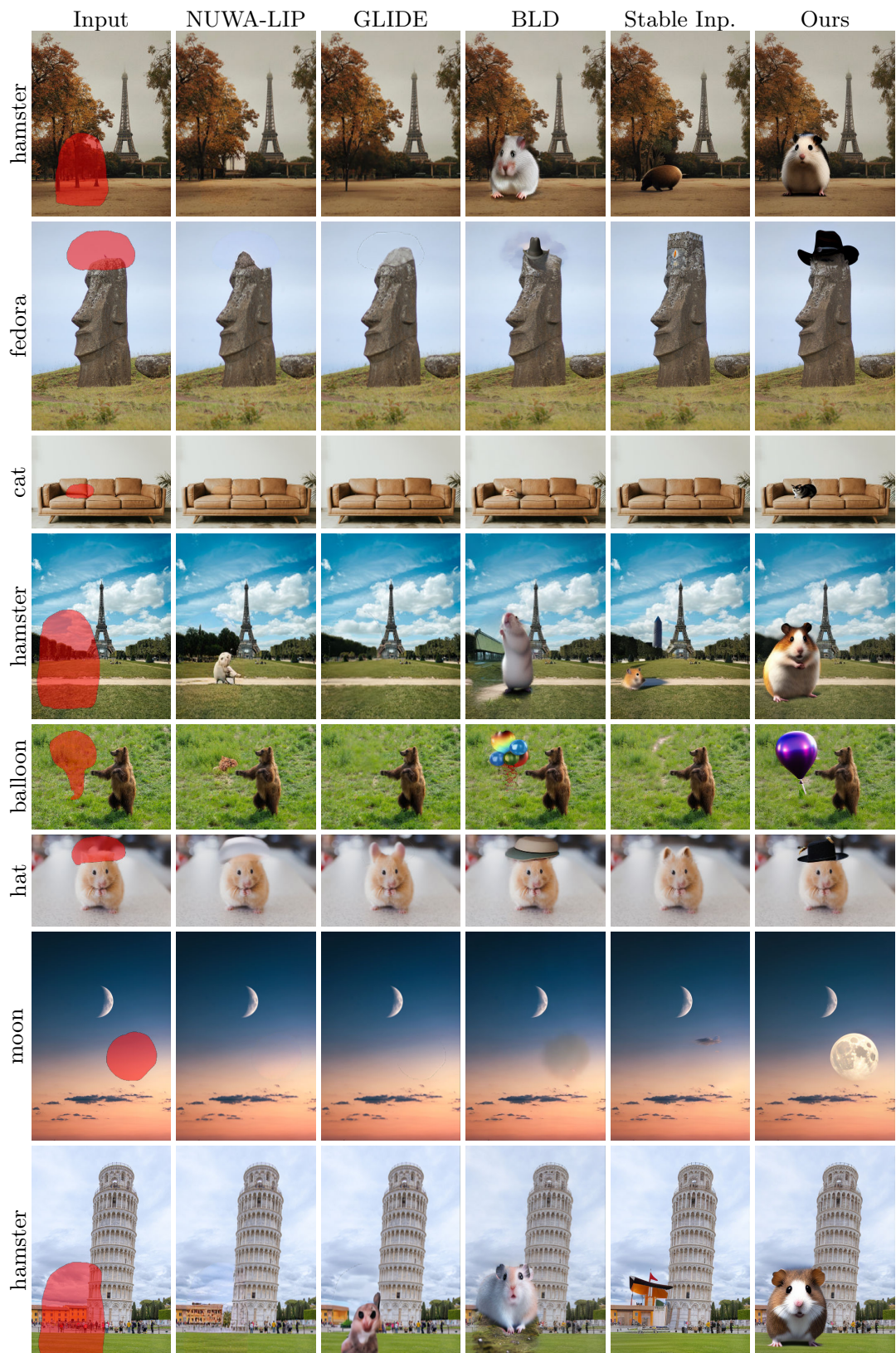


Figure 16. More qualitative comparison results. Zoom in to view high-resolution details.

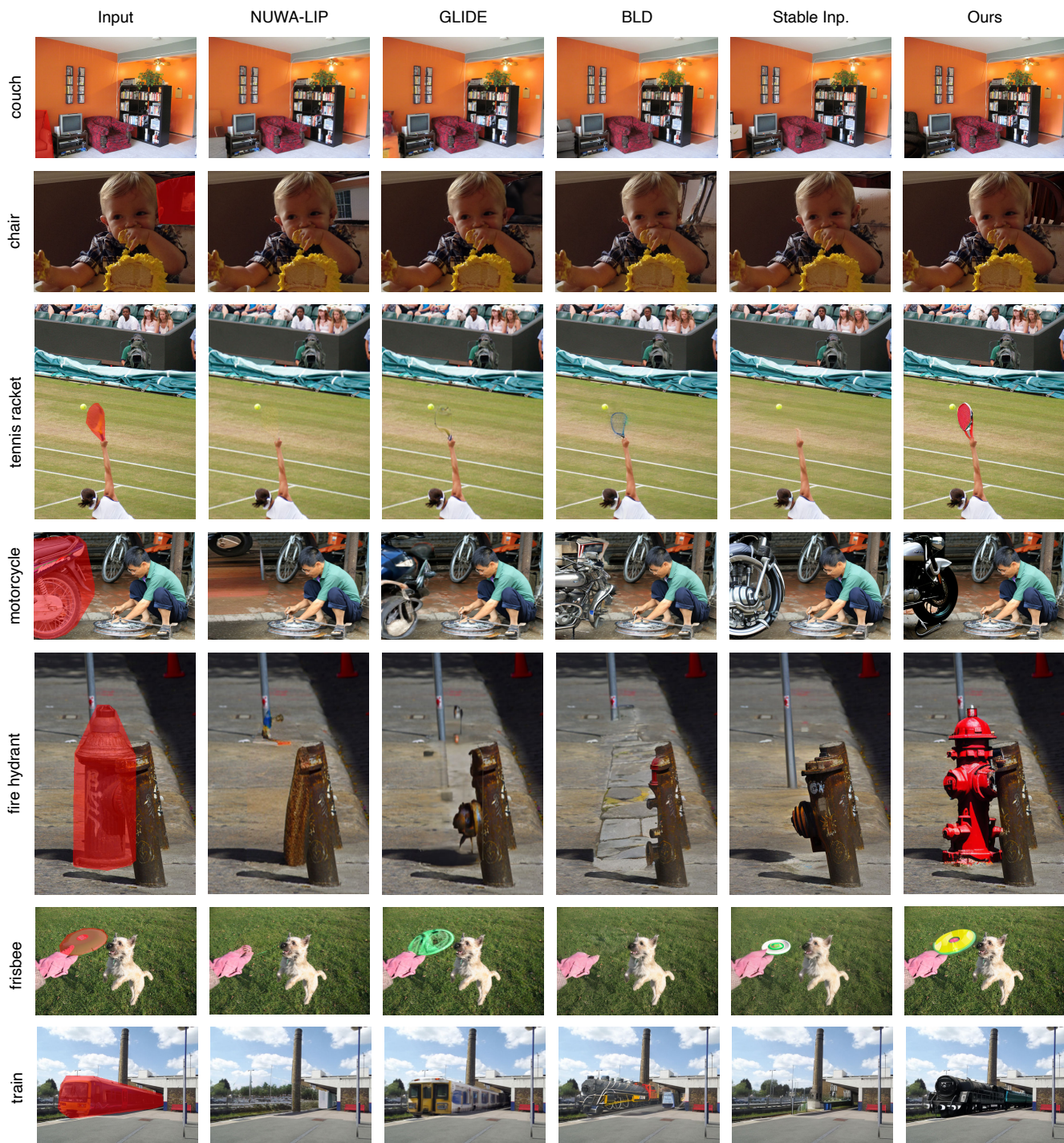


Figure 17. More qualitative comparison results on MSCOCO 2017.

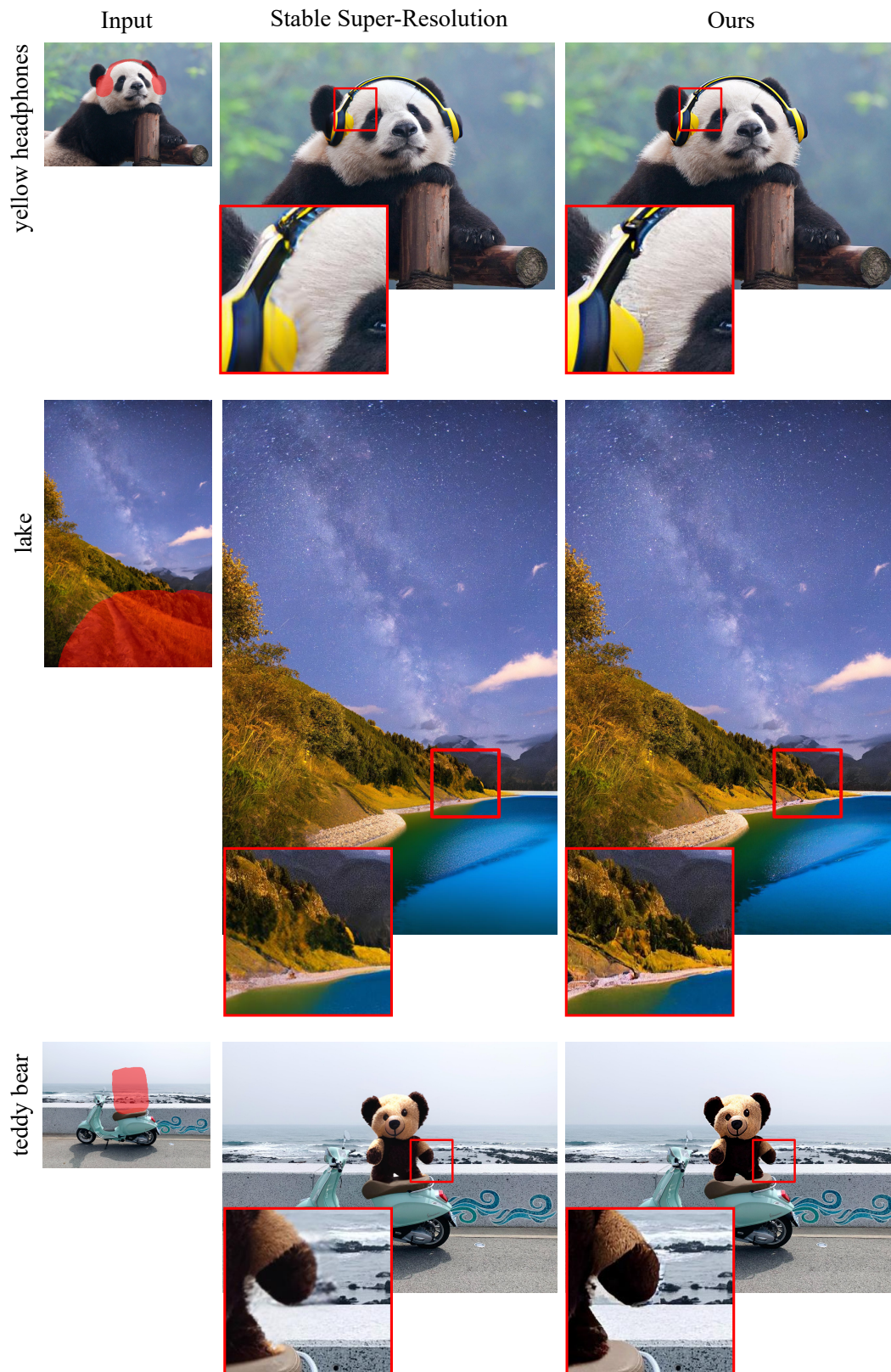


Figure 18. Comparison between vanilla SD 2.0 upscale and our approach. In all examples the large side is 2048px. The cropped region is 256x256px. Best viewed when zoomed in.

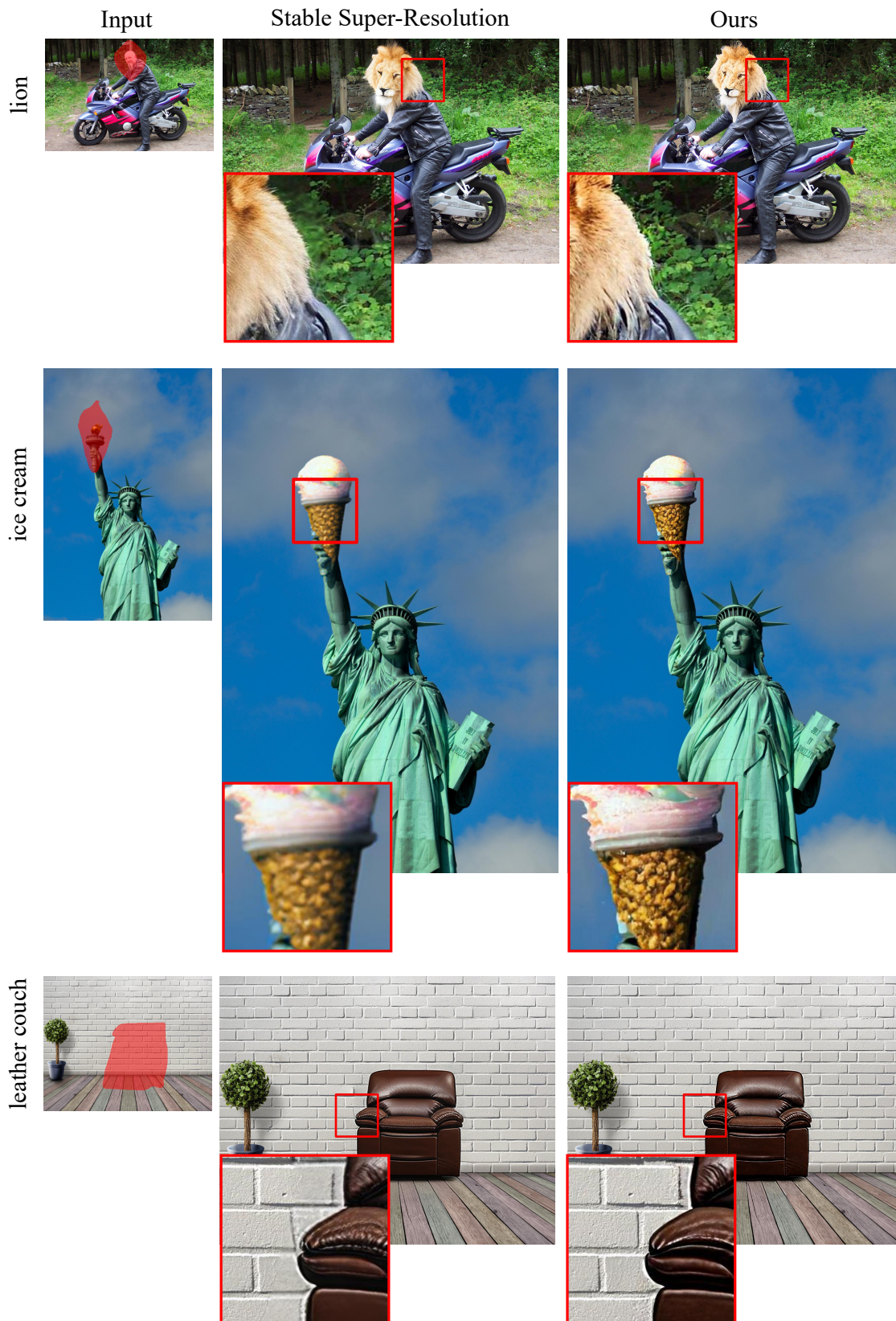


Figure 19. Comparison between vanilla SD 2.0 upscale and our approach. In all examples the large side is 2048px. The cropped region is 256x256px. Best viewed when zoomed in.



Figure 20. Competitor models have no issue generating the same object if an existing copy of it is removed



Figure 21. Comparison with baselines when generating more results from different seeds (1/3). Prompt: boat. Zoom in to view high-resolution details.

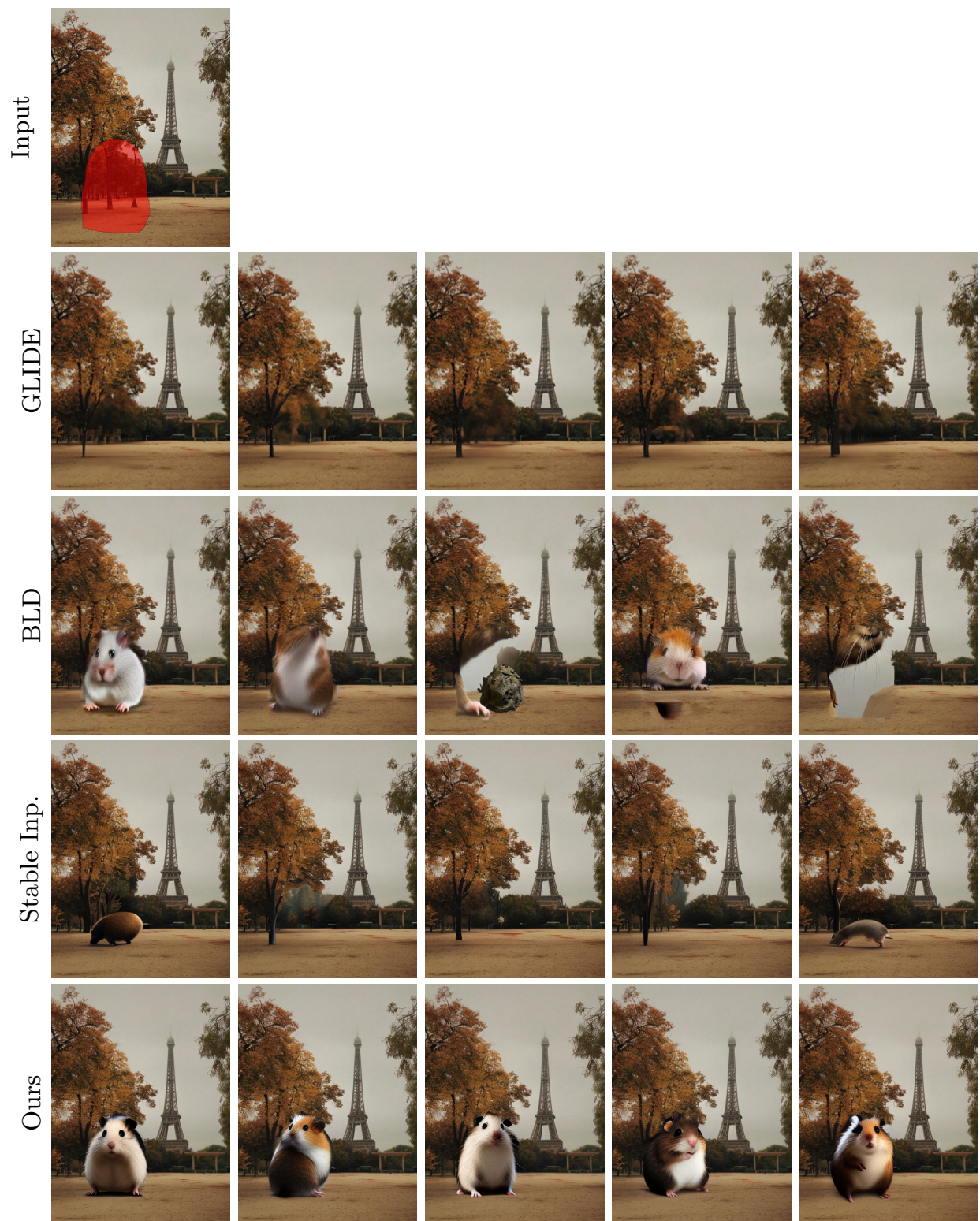


Figure 22. Comparison with baselines when generating more results from different seeds. (2/3). Prompt: hamster. Zoom in to view high-resolution details.



Figure 23. Comparison with baselines when generating more results from different seeds. (3/3). Prompt: dog. Zoom in to view high-resolution details.

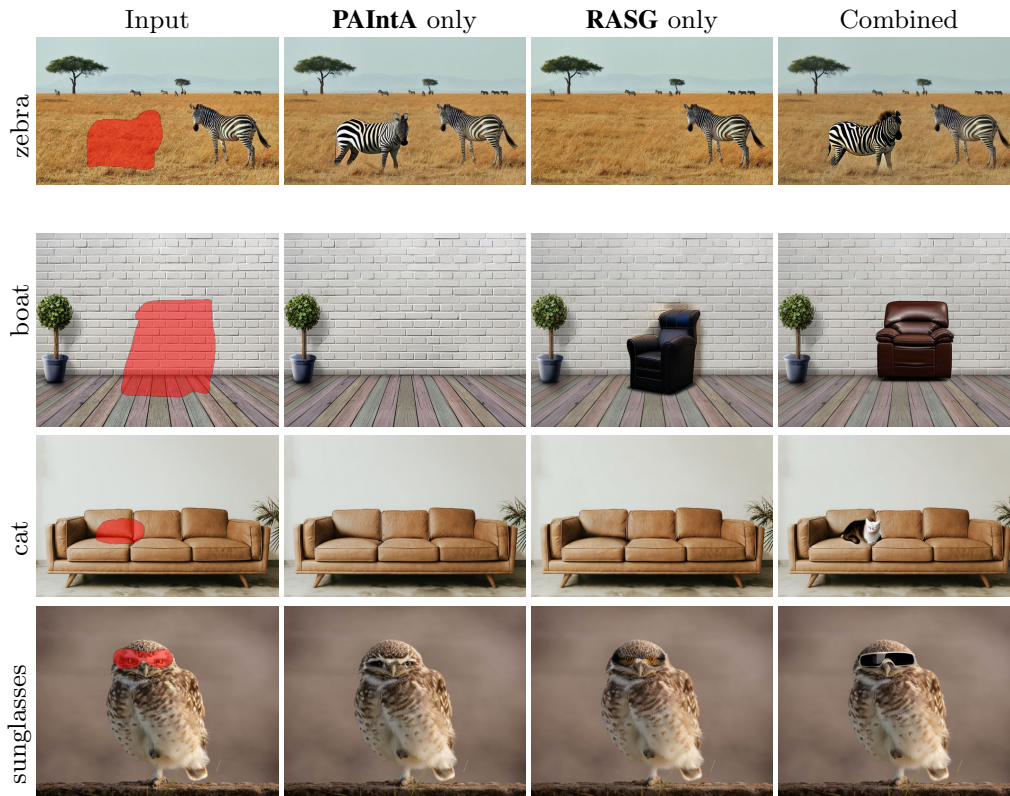


Figure 24. Ablation study of the visual results of our contributions RASG and PAIntA.

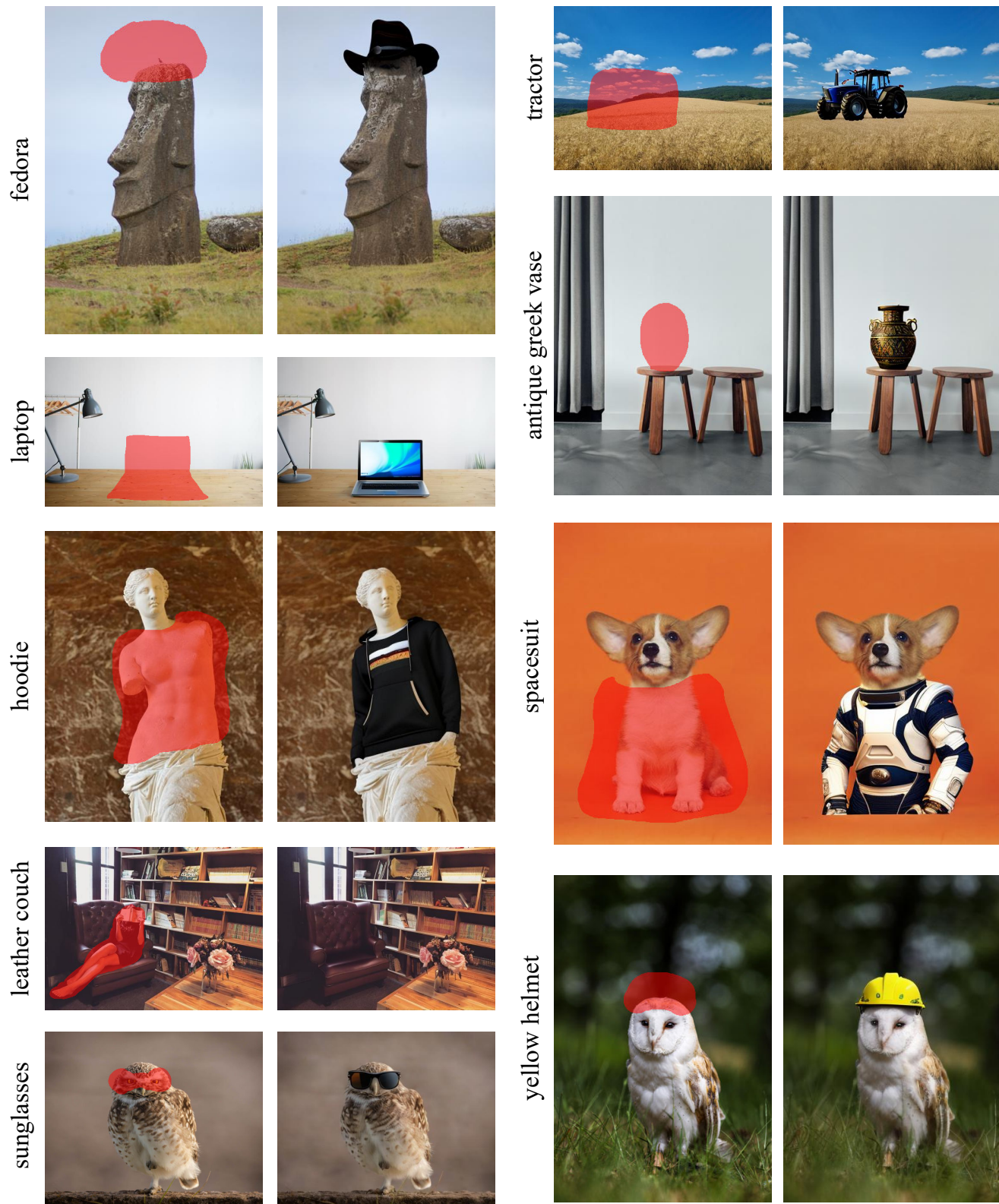


Figure 25. More results of our method.

boots



parrot



Figure 26. More high-resolution results of our method. Zoom in to view high-resolution details.

potted roses



raccoon



Figure 27. More high-resolution results of our method. Zoom in to view high-resolution details.

salad



castle



Figure 28. More high-resolution results of our method. Zoom in to view high-resolution details.